(4)

MARINE PHYSICAL LABORATORY

SCRIPPS INSTITUTION OF OCEANOGRAPHY

San Diego, California 92152

Large Aperture Array Measurements of the Vertical Ambient Noise Field

B. J. Sotirin and W. S. Hodgkiss

MPL TECHNICAL MEMORANDUM 411

MPL-U-26/89
July 1989

Approved for public release; distribution unlimited.

SECURITY CLASSIFICATION OF THIS PAGE

REPORT DOCUMENTATION PAGE

1a. REPORT SECURITY CLASSIFICATION UNCLASSIFIED	1b RESTRICTIVE MARKINGS
2a. SECURITY CLASSIFICATION AUTHORITY	3. DISTRIBUTION / AVAILABILITY OF REPORT Approved for public release; distribution unlimited.
2b. DECLASSIFICATION / DOWNGRADING SCHEDULE	
4. PERFORMING ORGANIZATION REPORT NUMBER(S) MPL TECHNICAL MEMORANDUM 411 [MPL-U-26/89]	5 MONITORING ORGANIZATION REPORT NUMBER(S)
6a. NAME OF PERFORMING ORGANIZATION Marine Physical Laboratory 6b. OFFICE SYMBOL (If applicable) MPL	7a. NAME OF MONITORING ORGANIZATION Office of Naval Research Department of the Navy
6c. ADDRESS (City, State, and ZIP Code) University of California, San Diego Scripps Institution of Oceanography San Diego, CA 92152	7b. ADDRESS (City, State, and ZIP Code) 800 North Quincy Street Arlington, VA 22217-5000
8a. NAME OF FUNDING / SPONSORING ORGANIZATION Office of Naval Research 8b. OFFICE SYMBOL (If applicable) ONR	9. PROCUREMENT INSTRUMENT IDENTIFICATION NUMBER N00014-87-K-0225; N00014-87-C-0127
8c. ADDRESS (City, State, and ZIP Code) Department of the Navy 800 North Quincy Street Arlington, VA 22217-5000	10. SOURCE OF FUNDING NUMBERS PROGRAM ELEMENT NO. / PROJECT NO. / TASK NO. / WORK UNIT ACCESSION NO.

11. TITLE (Include Security Classification)
LARGE APERTURE ARRAY MEASUREMENTS OF THE VERTICAL AMBIENT NOISE FIELD

12. PERSONAL AUTHOR(S)
B. J. Sotirin and W. S. Hodgkiss

13a. TYPE OF REPORT	13b. TIME COVERED	14. DATE OF REPORT (Year, Month, Day)	15. PAGE COUNT
tech memo	FROM _____ TO _____	July 1989	43

16. SUPPLEMENTARY NOTATION

17. COSATI CODES			18. SUBJECT TERMS (Continue on reverse if necessary and identify by block number)
FIELD	GROUP	SUB-GROUP	vertical array, ambient noise, directional spectral estimates

19. ABSTRACT (Continue on reverse if necessary and identify by block number)

Use of a large aperture vertical array allows investigation into the fine-scale structure of the directional ambient noise field. Frequency and directional spectral estimates are calculated during the passage of a local storm, providing a detailed study of ambient noise levels at low frequencies as wind speed increases from 2 m/s to 12 m/s over a 21 hour period. Spectral levels of horizontal beams reflect distant sources. Spectral levels of beams directed toward the surface and the bottom display a threshold type behavior, suggesting the abrupt onset of a source mechanism such as breaking waves. Subsequent thresholds may indicate a change in source mechanism such as the conversion from spilling breakers to plunging breakers.

20 DISTRIBUTION / AVAILABILITY OF ABSTRACT ☐ UNCLASSIFIED/UNLIMITED ☒ SAME AS RPT. ☐ DTIC USERS	21. ABSTRACT SECURITY CLASSIFICATION UNCLASSIFIED
22a. NAME OF RESPONSIBLE INDIVIDUAL W. S. Hodgkiss	22b TELEPHONE (Include Area Code) (619) 534-1798 22c. OFFICE SYMBOL MPL

DD FORM 1473, 84 MAR 83 APR edition may be used until exhausted. All other editions are obsolete

SECURITY CLASSIFICATION OF THIS PAGE

☆ U.S. Government Printing Office: 1986—607-044

Large Aperture Array Measurements of the Vertical Ambient Noise Field

B. J. Sotirin and W. S. Hodgkiss

Marine Physical Laboratory
Scripps Institution of Oceanography
University of California, San Diego
La Jolla, CA 92093

ABSTRACT

Use of a large aperture vertical array allows investigation into the fine-scale structure of the directional ambient noise field. Frequency and directional spectral estimates are calculated during the passage of a local storm, providing a detailed study of ambient noise levels at low frequencies as wind speed increases from 2 m/s to 12 m/s over a 21 hour period. Spectral levels of horizontal beams reflect distant sources. Spectral levels of beams directed toward the surface and the bottom display a threshold type behavior, suggesting the abrupt onset of a source mechanism such as breaking waves. Subsequent thresholds may indicate a change in source mechanism such as the conversion from spilling breakers to plunging breakers.

Large Aperture Array Measurements of the Vertical Ambient Noise Field

B. J. Sotirin and W. S. Hodgkiss

Marine Physical Laboratory
Scripps Institution of Oceanography
University of California, San Diego
La Jolla, CA 92093

INTRODUCTION

To measure low frequency (20 - 200 Hz) vertical directionality of the oceanic ambient noise field requires a long array of hydrophones. Initial vertical directionality investigations were at high frequencies (near 1 KHz) with shorter arrays [Anderson, 1958; Rudnick and Squier, 1967]. These measurements showed a non-uniform spatial distribution with more noise in vertical directions than in horizontal directions due to a dominance of local environmental noise sources at high frequencies. Initial low frequency measurements provided a general spatial distribution description of ambient noise and its variation with wind speed [Fox, 1964; Axelrod *et al*, 1965]. Omnidirectional spectral measurements indicated that ship noise dominates the environmental noise in this frequency region, and the directional measurements showed that more noise arrives from the horizontal than from the vertical, a reversal of the patterns characteristic of high frequencies.

More recently, the spatial distribution of ambient noise at low frequencies has been described as a broad pedestal of energy arriving between ±20° of horizontal in the deep sound channel [Anderson, 1979] with levels up to 25 dB above the higher angle levels. Ray tracing showed that the surface interacting rays which would contain ship noise, arrive within a narrow band of angles around ±12° to ±15°. This implied that the low frequency spatial distribution in a range independent environment should have a double-humped pattern with the width of the notch between the humps decreasing with depth [Cavanagh and Renner, 1980]. Yet measurements showed a pedestal with broad frequency and spatial characteristics, although the pedestal width did decrease with depth.

Two mechanisms were suggested by Anderson [1979] to account for the additional noise at near horizontal angles: (1) high latitude ducting, based on the shallower sound speed minimum at high latitudes and (2) down slope conversion (or the slope enhancement effect), based on on sloping bottom reflection. These mechanisms would convert noise traveling at near vertical angles to horizontal angles so that it travels with low loss in the deep sound channel, filling in the predicted noise notch. Initially the idea of slope-converted ship dominated spectra directed the investigations. The downslope conversion of noise from ships driving over seamounts and the continental slope was discussed by Morris [1975] and later by Wagstaff [1981] who emphasized the importance of directional measurements since the omnidirectional measurements of a single hydrophone may be dominated by the horizontal component. More recently, ducted transmission and wind generated mechanisms have gained more prominence. Three models of ocean noise were considered by Dashen and Munk [1984]: scattering, downslope

conversion and ducted transmission from high latitudes; the effect of scattering was shown to be too weak to be effective and although these authors preferred the ducting process on a physical basis, they concluded that the shipping density at high latitudes was insufficient to produce the absolute levels measured, and that continental slope conversion was the most probable mechanism by default. The significance of high latitude winds was discussed by Bannister [1986] who estimated the contributions arriving horizontally from ducting and downslope conversion of wind noise, and concluded that ducting of high latitude winds could produce horizontal levels comparable to those of downslope converted ship noise.

Experimental verification of these mechanisms is difficult due to the obstacles encountered in separating the sources and source mechanisms. Experimental evidence of ducted wind generated noise [Bannister, 1986] was based on interpretation of vertical noise distributions in the low shipping density areas near New Zealand, measured by Browning *et al* [1982] and Burgess and Kewley [1983] which were similar to those measured in the high density shipping regions of the North Pacific. Burgess and Kewley [1983] found significant wind dependencies at frequencies from 37 to 800 Hz, however it was not conclusively shown that the wind dependencies were a ducted or converted effect rather than a local effect. Experimental verification of slope-converted ship generated noise was reported by Wales and Diachok [1981] at a site bathymetrically shielded from contamination of high latitude ducting effects, by Carey [1986] using a towed narrowband source and by Hodgkiss and Fisher [1987] who present decreasing noise magnitude results as a function of range from the California coast. Downslope conversion has been accepted as a mechanism for translating surface generated noise to the deep sound channel, however the existence of the pedestal structure in the vertical directionality from low shipping density areas suggests a major energy source is that of distant storms.

Local storm energy has been shown to contribute to the ambient noise field as well. Storm induced noise has been observed at high frequencies as the spectral levels increase with wind speed. At low frequencies however, there is no consensus regarding the extent of the wind induced effects. Efforts to conform to the logarithmic dependencies seen at high frequencies has led to a variety of predicted low frequency spectral levels [Urick, 1984]. Difficulties arise in estimating the "wind dependent portion" [Crouch and Burt, 1972] of an omnidirectional signal which may be affected by other sources. An obvious experimental approach is the use of the directional capabilities of an array, however, previous measurements [Burgess and Kewley, 1983; Hodgkiss and Fisher, 1987] introduced additional parameters in terms of variations in location and time which complicate interpretation of wind induced effects.

The advent of large aperture arrays with many elements provide measurements of ambient noise characteristics with high resolution. In this report, use of a large aperture array equipped with an acoustic navigation system which allows array shape estimation, enables study of ambient noise fine-scale structure. The array, deployed from Research Platform *FLIP* which was moored in the NE Pacific, was positioned at three nominal depths covering the water column from 400 m to 3100 m with 7.5 m sampling increments The 900 m array aperture produced a 1° beam at 100 Hz. A detailed estimate was obtained of the vertical spatial variability of ambient noise as wind speed increased from 2 m/s to 12 m/s over a 21 hour period.

Previous work indicated that the array shape may be estimated as straight and nearly vertical, moving for the most part like a simple pendulum [Sotirin and Hildebrand, 1989]. Array calibration showed that specific channels may be limited

by system noise and should be avoided, however the accumulated effect of these channels does not contaminate the directional spectral levels [Sotirin and Hodgkiss, 1989].

The present work is presented in three sections. Preliminary statistical test results, reported in Section I, show that ambient noise data consist of independent samples of normally distributed processes which are stationary over limited time periods. Temporal variability of ambient noise is studied to assist in comparisons of data recorded at different times. Issues of spectrum restoration, beamformed sidelobe leakage and angular resolution are discussed in Section II. Ambient noise spectral levels, presented in the last section, are compared to previous measurements. The small noise level variation with depth, the shape of the spatial distribution and deviations with respect to frequency, time and wind speed are presented. A fine scale analysis of ambient noise during the passage of a local storm is shown.

1. TEMPORAL VARIABILITY

This section describes the temporal variability of ambient noise as a prerequisite to data processing and interpretation. The ambient noise field is analyzed for independence and time stationarity. Earlier investigations indicated that the time period of fluctuation depends upon the mechanism generating the noise; measurements above 150 Hz correspond to weather patterns whereas noise measurements between 20 and 150 Hz correspond to the proximity, density and speed of ship traffic [Jobst and Adams, 1977]. Our results show that complex narrowband samples at 75 Hz, a ship dominated frequency, are independent and Gaussian with stationarity lengths longer than previously reported (3 minutes at high wind speed [Arase and Arase, 1968] and 22 minutes at unreported wind speed [Jobst and Adams, 1977]. The underlying processes create an ambient noise field which varies with ship distribution, speed and density, and with environmental parameters such as wind speed and sound speed profile. The mean distribution is modulated by small scale variations which impose a limit on the significance of measurement deviations. The variance of ambient noise spectral measurements increases with the length of time between samples, even for constant array depth, wind speed and time of day.

1.1. Statistical Tests

Statistical tests were used to analyze ambient noise data for independence, stationarity and normality. The test data consisted of sequential complex spectral estimates at 75 Hz every second (1.024 s) over a 50 minute interval for each of the 120 array channels. The estimates were calculated with a 1 Hz bandwidth from 512 data samples windowed with a Kaiser-Bessel function (α = 2.5). Two data segments were selected: (1) local wind speed of 4 kts (Julian day 268, GMT 1010 where GMT is Greenwich Mean Time) with the array deployed vertically between 2200 m and 3100 m and (2) local wind speed of 20 kts (Julian day 258, GMT 1437) with the array deployed between 400 m and 1300 m.

Sample independence was determined using the nonparametric runs test based on pair-wise deviations [Middleton, 1969]. Sequential sign consistent values, calculated as the difference between sequential sample pairs, constitute a run. If the narrowband process at a sensor is $A(t)\cos(\omega t + \phi(t))$ and the inphase and quadrature components are $I(t) = A(t)\cos\phi(t)$ and $Q(t) = A(t)\sin\phi(t)$

respectively, then the pairwise values employed in the runs test are $SGN[I(t) - I(t+1)]$, and $SGN[Q(t) - Q(t+1)]$, where t is incremented (δt = 2 s) over the data segment. The number of runs then is illustrated by example; i.e. +++--++---+----++ has r=7 runs, M_1=8 positive values, M_2=9 negative values, and M=17 values. If the data are independent observations of the same random variable then, for large M (M > 40), r is a normally distributed random variable with a mean and variance of [Bendat and Piersol, 1971]:

$$\mu_r = \frac{2M_1M_2}{M} + 1; \qquad \sigma_r^2 = \frac{2M_1M_2(2M_1M_2 - M)}{M^2(M-1)}; \qquad Z_s = (r - \mu_r)/\sigma_r$$

where Z_s is the test statistic. The test statistic Z_s is a zero mean Gaussian random variable which is tested against an apriori determined threshold Z_α, where α is the significance level. The null hypothesis for this test is that the M observations are independent samples of the same random variable. If $Z_s \leq Z_\alpha$ then the null hypothesis is accepted at the α level of significance. The data segments for this test were each 50 minutes long (M > 4000) and results for the 0.05 and 0.1 significance levels were calculated. The significance level is the probability that the null hypothesis will be rejected when the segment is independent; at the 0.1 level of significance, 90% of the segments should pass. Inphase and quadrature components for each array channel result in 240 data segments, so at the 0.1 level of significance, 24 test results would be falsely rejected and at the 0.05 level of significance, 12 test results would be falsely rejected. At low and high wind speeds, 18 and 24 segments failed the test at the 0.1 level of significance level respectively, and 10 failed at the 0.05 level of significance, showing that the data are independent.

The stationarity time length was determined by the Kolmogorov-Smirnov two-sample test. This method used the cumulative distribution function (CDF) of the data (Figure 1) which is the fraction of samples whose amplitudes are less than a specified value. Procedurally, the data segment is divided in half and the CDF is calculated for each half. The Kolmogorov-Smirnov test statistic is the maximum value of the absolute difference between the two CDF's:

$$z_{sample} = max|F_{x_1}(x) - F_{x_2}(x)|.$$

The null hypothesis is that the two data sets belong to the same distribution. If $z_{sample} \leq z_\alpha$ then the hypothesis is accepted at the α level of significance. For a large number of data points (N>20), the significance level of the test statistic z_{sample} is [Press, *et al*, 1986]

$$Q_{KS}(z_\alpha > z_{sample}) = Q_{KS}(\lambda) = 2\sum_{j=1}^{\infty}(-1)^{j-1}\, e^{-2j^2\lambda^2},$$

$$\text{where } \lambda = \sqrt{\frac{N_1N_2}{N_1 + N_2}}\; z_{sample}$$

The significance level was calculated for the inphase and quadrature components of each array channel over time periods of 20, 30, 40 and 50 minutes (Figure 2).

The results are different for the two data segments. The low wind speed segment is stationary at the 5% level of significance for up to 50 minutes. At 60 and 70 minutes, the number of individual test which fail is still less than 9% at the

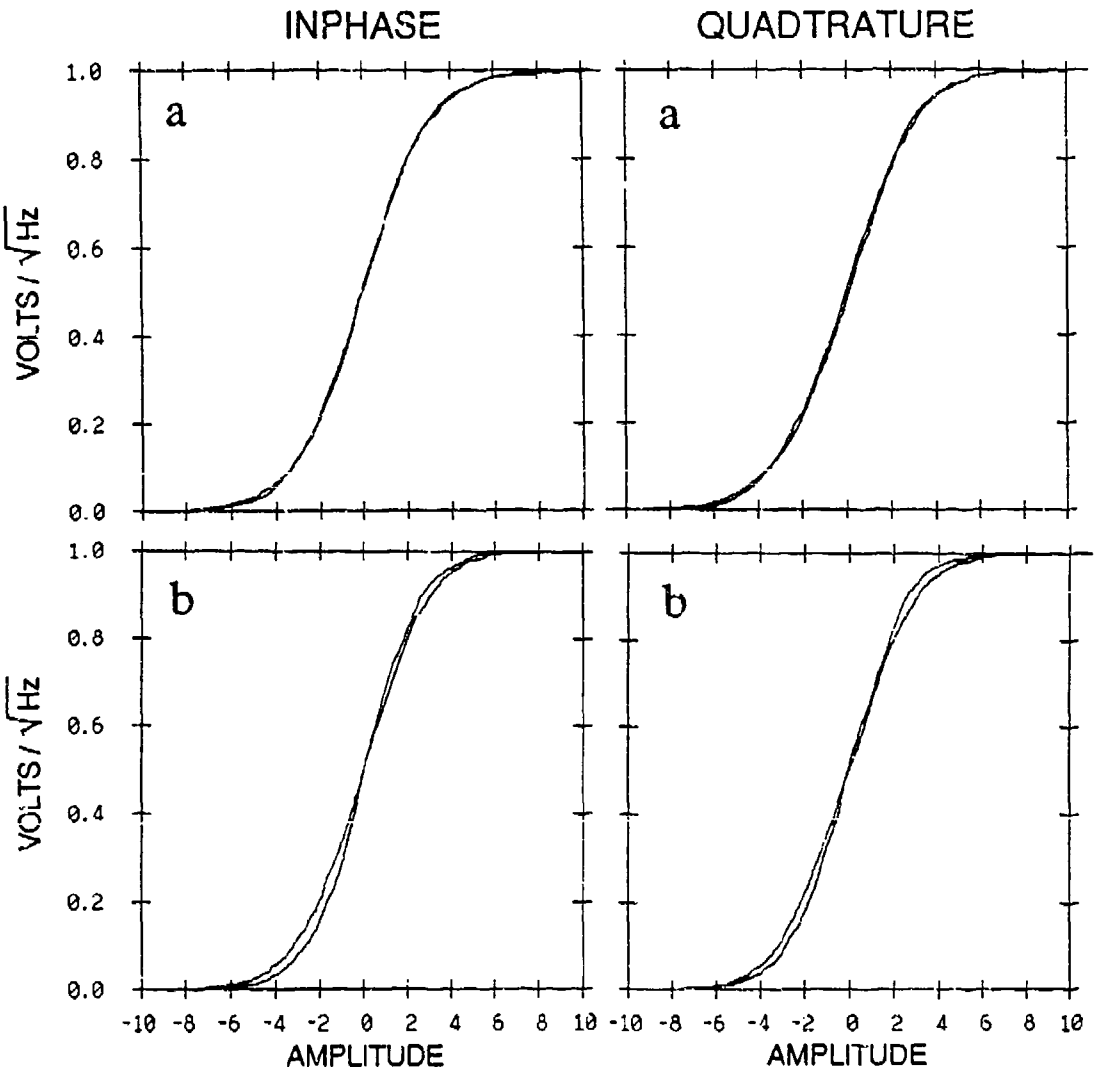

Figure 1 Cumulative distribution two-sample test. The results of the Kolmogorov-Smirnov two-sample test are shown for the inphase and quadrature components of array channel 23 for a 50 minute time segment at 75 Hz. The segment on top (a) is accepted as being stationary at the 0.05 level of significance. This segment was recorded during a low wind condition (2 m/s) and the array was deployed nominally to 2650 m. The segment on the bottom (b) fails at the 0.05 level of significance; 10 m/s winds prevailed and the array was deployed at a nominal depth of 850 m. The Julian day (Jday) and Greenwich mean time (GMT) are indicated.

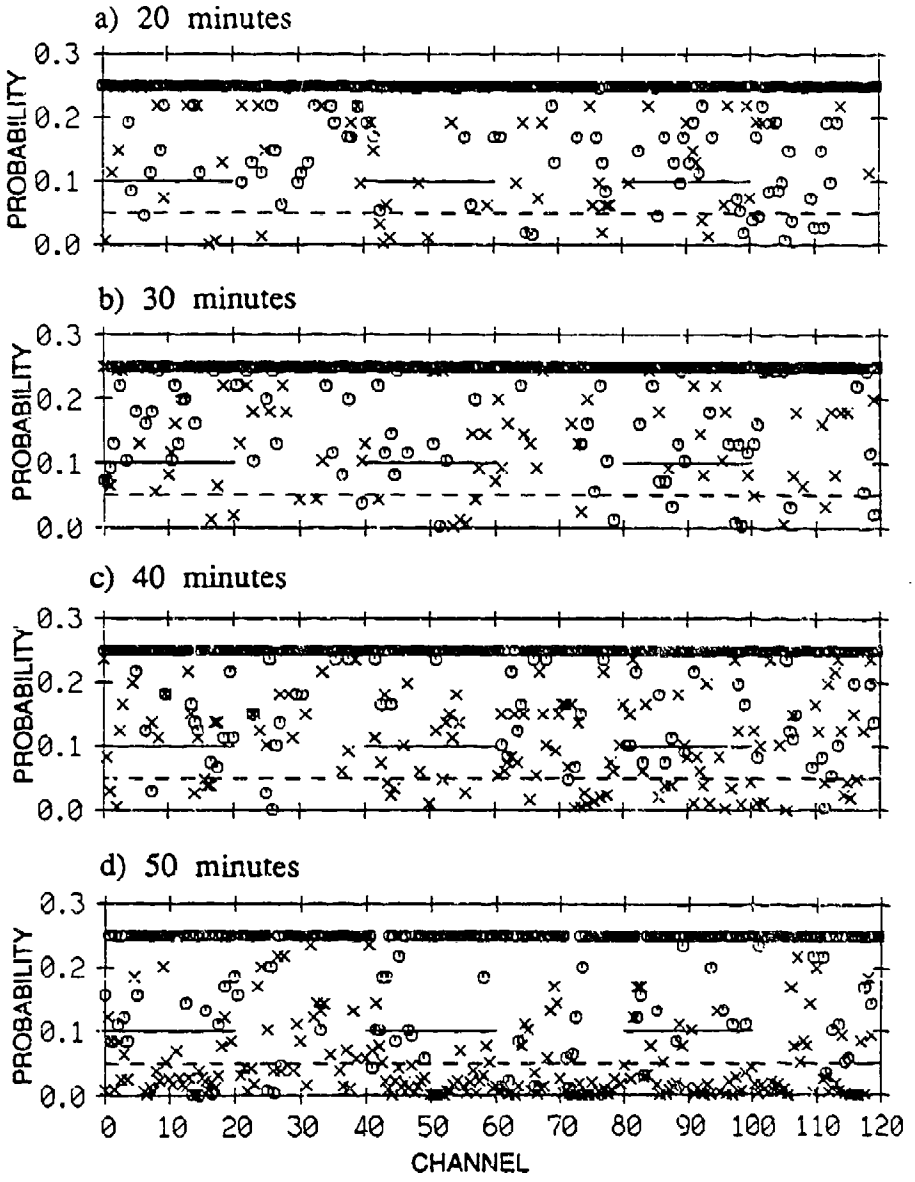

Figure 2 Data stationarity. The probability α of the observed test statistic is shown for the in-phase and quadrature components of each array channel. The o's represent the low wind speed data segments; the x's represent the high wind speed data segments. The 0.05 level of significance is shown with small dashed lines; the 0.1 level of significance is shown with large dashed lines. Probabilities greater than 0.25 were clipped for illustrative purposes. Interpretation of this data is such that any test result represented as an x or o which is less that a specified probability fails at that level of significance; e.g. the null hypothesis that the two data segments have the same distribution is rejected at the 0.05 level of significance for any result which is less than 0.05.

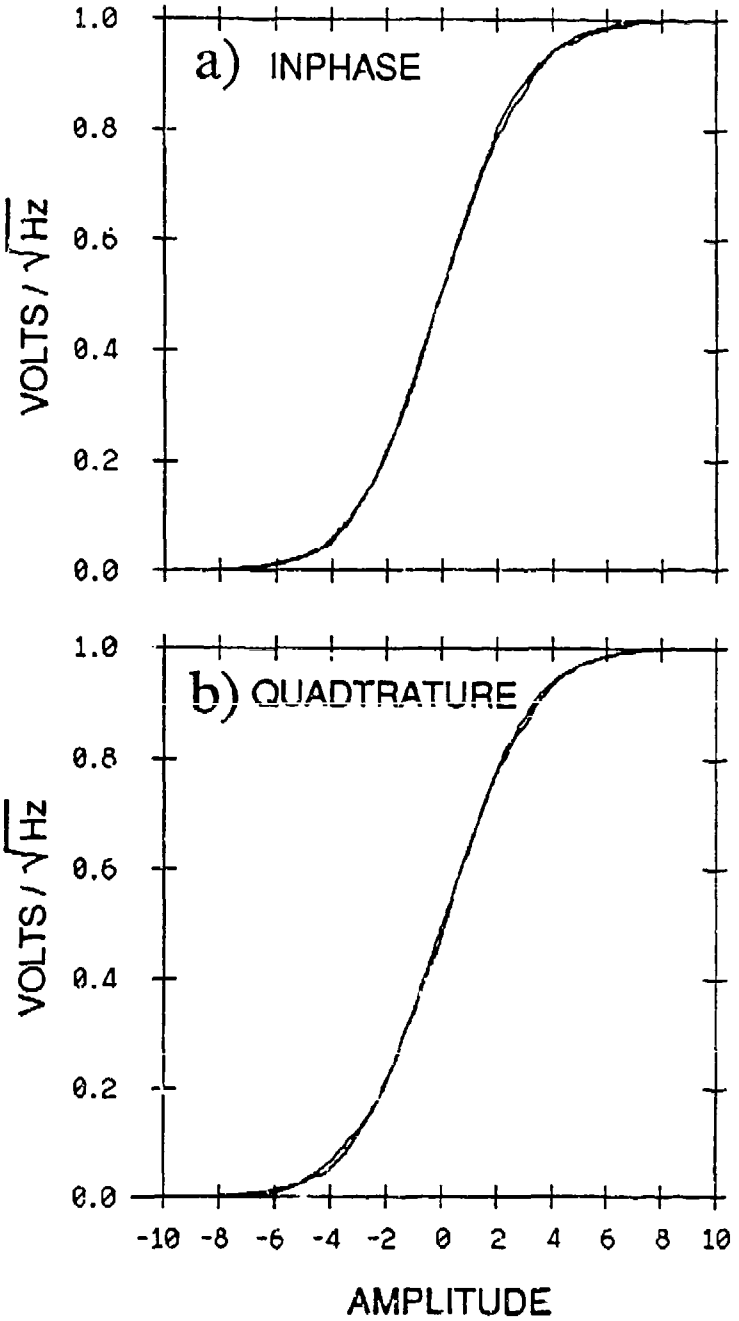

Figure 3 Cumulative distribution one-sample test. The Kolmogorov-Smirnov one-sample test results are shown for the 75 Hz inphase (a) and quadrature (b) components for array channel 23 and a Gaussian distribution with the same mean and variance as the data segment. The data was from the high wind speed segment. The sample mean and variance for the inphase segment was 6.70 and 7.67, respectively. The sample mean and variance for the quadrature segment was 0.157 and 7.70, respectively. Data segment lengths of 20, 30 and 40 minutes also passed.

0.05 level of significance. For the high wind speed segment however, the stationarity hypothesis is accepted at the 0.05 level of significance for a segment length of 20 minutes, but fails by a narrow margin (5.42%) at 30 minutes with the number of failures increasing significantly above 30 minutes.

The hypothesis that the data components are normally distributed is tested using the Kolmogorov-Smirnov one-sample test. The procedure is similar to the two-sample test with the test statistic z_{sample} defined as the maximum difference between the experimental cumulative distribution and that of a normally distributed function with the same mean and variance as the data segment. The null hypothesis that the inphase and quadrature components of the narrowband noise are normally distributed is accepted at the α level of significance if $z_{sample} \leq z_{\alpha}$. The probability that $z_{sample} \leq z_{\alpha}$ is calculated from the equation above with $\lambda = \sqrt{N} z_{sample}$, where N is the number of data samples in the segment. Although the probability is defined for an apriori determined theoretical distribution, use of the data sample mean and variance leads to a more conservative test by decreasing the observed test statistic [Middleton, 1969]. The cumulative distribution functions for array channel 23 and the Gaussian distribution with sample mean and variance are shown in Figure 3. The hypothesis was accepted for the inphase and quadrature components for both the high and low wind speed segments at the 0.05 level of significance.

There appears to be a local wind speed dependence in the stationarity results (Figure 2). However, additional data samples were not available to corroborate this hypothesis, and due to the difference in array depth during the recording of the samples, a wind dependence can not be substantiated without further analysis. Although these tests were conducted over only a few data segments, it is assumed that under similar conditions, the data segments used in the ambient noise analysis may be considered independent, stationary and normally distributed.

1.2. Spectral Estimate Variability

In many investigations, the variation in ambient noise due to specific processes requires that the noise field be sampled at different times. For instance, to investigate ambient noise versus wind speed, the data recorded at specific wind speeds but at different times are compared. The mean spectral level is a not solely a function of wind speed and an estimate of the small scale variability is required to ascertain the significance of changes in wind speed. This variability is a combination of spatial and temporal interference patterns across the array during the sampled interval.

To estimate the variability of ambient noise spectral values with time, spectral estimates at 75 Hz were calculated from data recorded during similar environmental conditions and at approximately the same time of day. Squared magnitude estimates over a 22 minute interval were averaged, calibrated [Sotirin and Hodgkiss, 1989] and plotted for each array channel at 75 Hz. The data were selected to be free of any known nonstationary effects (e.g. seismic profiler, large strum amplitudes, nearby ships) with the expectation that the spectral level would vary smoothly across the array. A regression fit to the data across the array (whose mean level varies little with depth) was subtracted leaving channel deviations. The difference between the channel deviations taken at different points in time is illustrated in Figure 4 where increasing variability across the array is seen with increasing time lengths. This increase is quantified by calculating the

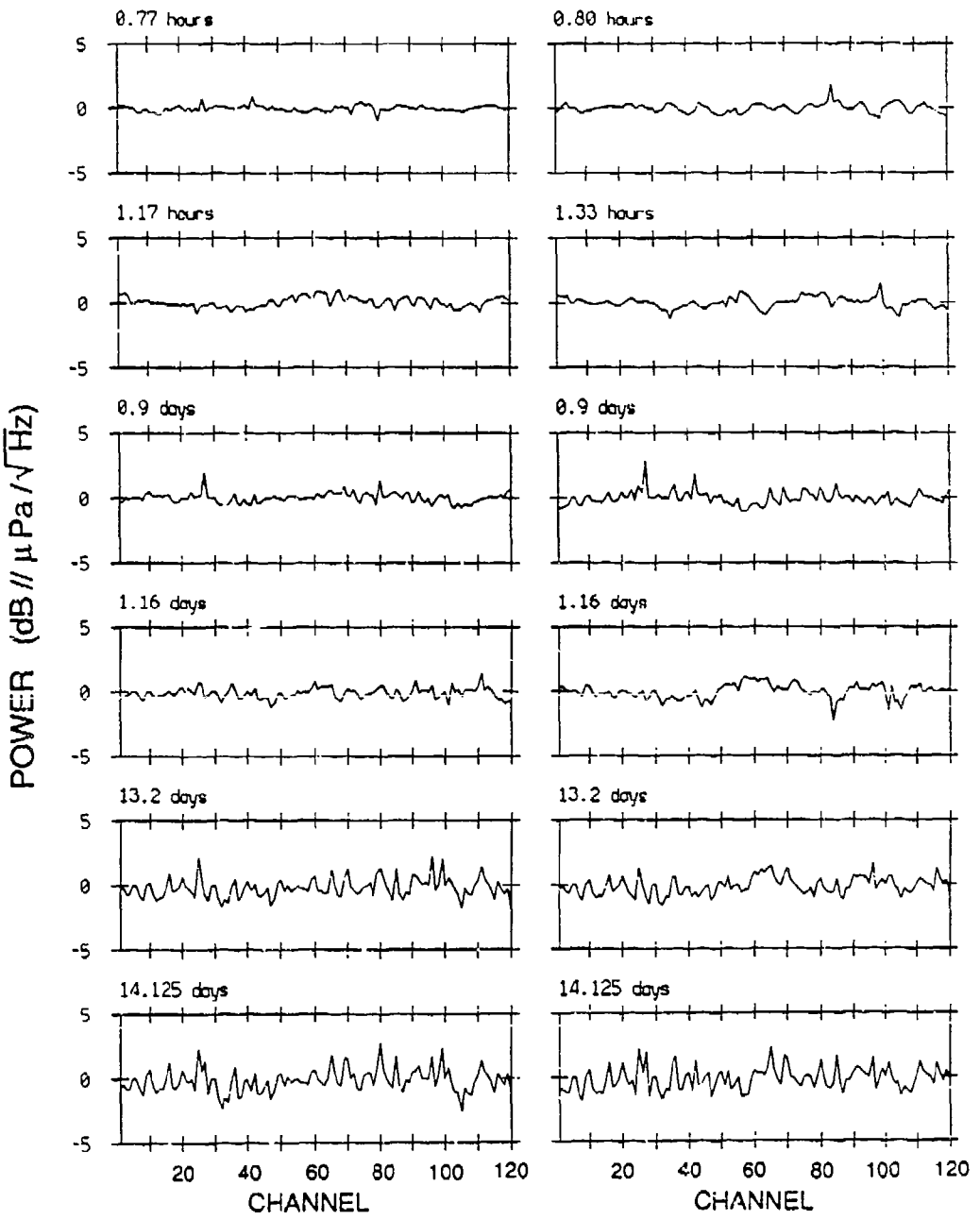

Figure 4 Variability of ambient noise spectral levels across the array. Spectral deviations as a function of time were differenced to investigate temporal variability across the array. The panels represent the channel to channel variation of spectral estimates separated in time by the amount shown above each panel. The spectral estimates were generated by incoherently averaging the squared magnitude FFT outputs for each array channel. The input segments were 50% overlapped, Kaiser-Bessel windowed (α=2.5), 1 second time series resulting in 2583 estimates of 0.98 Hz bin width. Each data sequence was 22 minutes in length and the results were plotted in dB re μPa√Hz. The 95% confidence interval of the estimates is +0.166 dB, -0.162 dB.

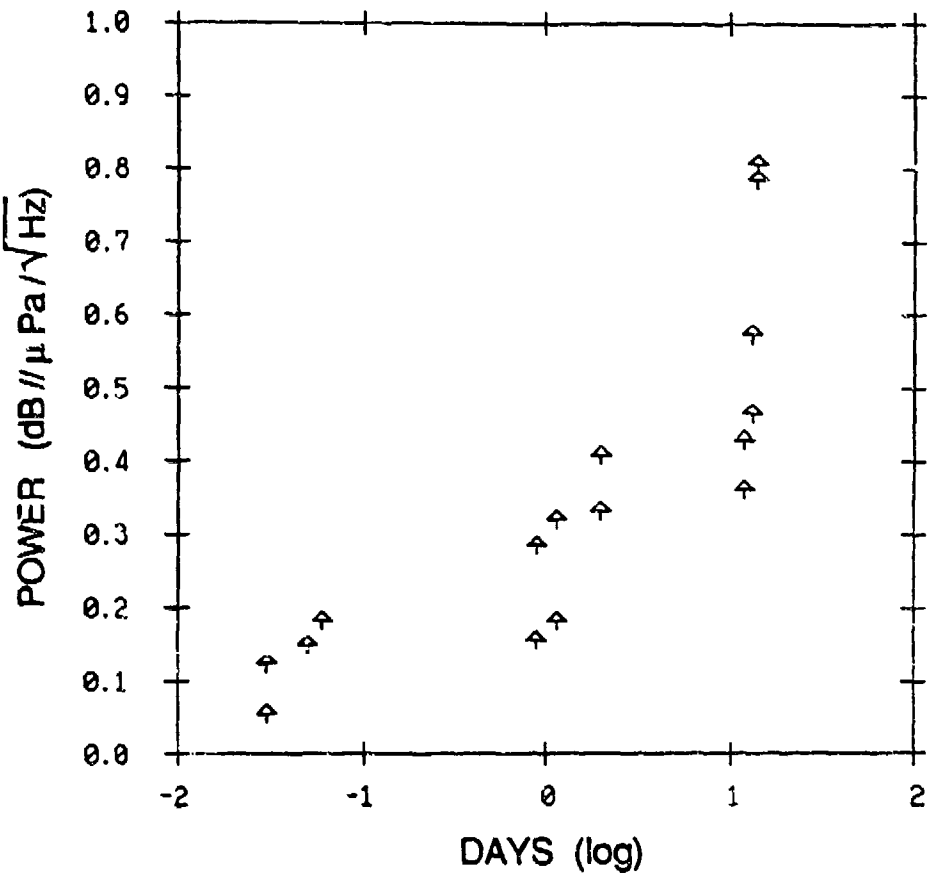

Figure 5 Variance as a function of time. The variance across the array of the spectral estimate differences is plotted as a function of the logarithm of the time difference.

variance across the array for each of the data segment pairs, and is plotted as a function of the logarithm of the time difference in Figure 5, demonstrating time variability of the ambient noise field. Although a sparse sampling is presented, a definite increase of variance is observed with time. Differences in spectral measurements taken at different times or at different spatial locations which are about 1 dB, could be due to either temporal and/or spatial variability of the source mechanisms in force.

2. INTERPRETING BEAMFORMED DATA

An acoustic array is a collection of hydrophones at discrete points in space whose outputs may be coherently combined in the beamforming process to estimate the directional spectrum of the ambient noise field. Use of such an array produces a distorted picture of the true directional spectrum, which may be discussed as two separate artifacts. The first is attributable to the discrete sampling of a continuous process, yielding limitations in wave number magnitude and spatial aliasing at frequencies above f = c/2d where c is the propagation speed and d is the array element spacing. The second is attributable to the spatial response of the array (a function of the array aperture) which bounds the angular resolution in vertical angle of arrival. If the array response (beampattern) were represented by an impulse function, then the beamformer output would accurately reflect the actual noise field input. This is not the case for the array considered here whose weighted spatial characteristics, due to finite length and limited number of elements, are described by a main beam of non-zero width which varies with frequency, and sidelobe levels between -30 and -40 dB.

The array beampattern is a spatial filter which is convolved with the true noise field to produce the estimated spatial spectrum. The Fourier transform of the beampattern illustrates the angular resolution of the array and is shown for 55 Hz in Figure 6. The estimated spectrum has a band limited angular response because the angular resolution is band limited. The zero crossing of the beampattern, known as the critical angle ϕ_c [Bracewell and Roberts, 1954], is pproximated by $\frac{\lambda}{\Gamma}$ where λ is the wavelength and Γ is the array aperture. The critical angle for the specific range of wave lengths considered here varies from 0.112 to 0.013 requiring a minimum sampling interval of 0.056 to 0.0065 radians (3.21 to 0.37 °) which is satisfied by the 512 point transforms discussed in the next section.

Recognizing the limitations of the array, various approachs have been suggested to estimate the true noise field, assuming that the array response function is independent of steering direction and is well known [Bracewell, 1958; McDonough, 1975]. These methods are constrained by the nonuniqueness of the solution, numerical difficulties, processing artifacts and uncertainty in the array beampattern response. A technique known as successive substitution [Bracewell and Roberts, 1954] was applied to samples of the measured ambient noise field at various frequencies to ascertain the gross effects of the array as a measurement system. An alternative to the restoration scheme in determining the limits of array distortion is that of a more controlled environment in which the "true" noise field, completely determined apriori, is convolved with the estimated array beampattern and compared to the measured data. Simulations indicate a sensitivity to array sidelobe structure under certain conditions, consequently absolute levels outside the ambient noise pedestal, must be viewed with regard to the parameters discussed below.

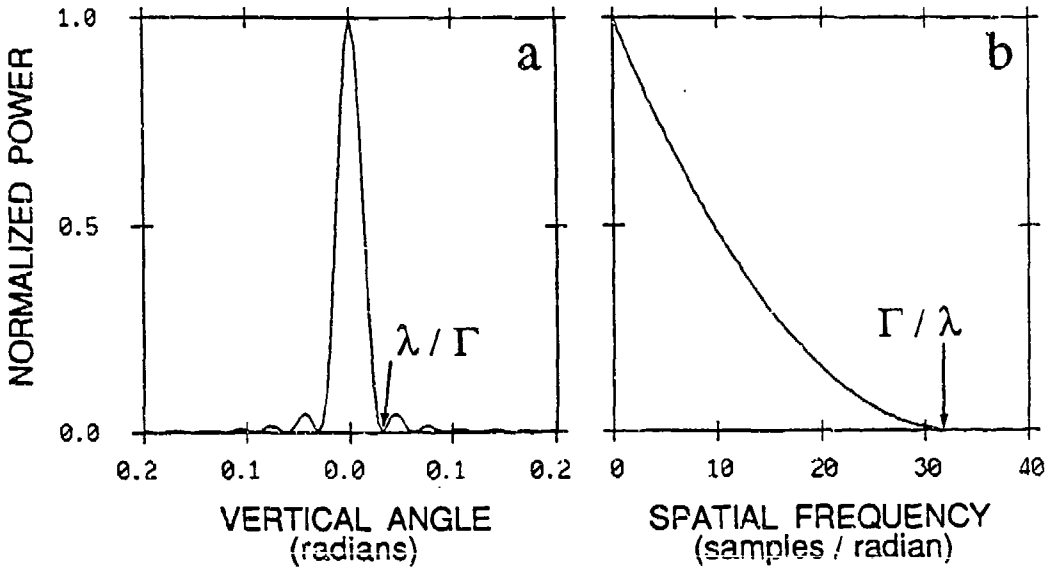

Figure 6 Angular resolution of the array. The theoretical array beampattern at 55 Hz is shown (a) for physical angles in normalized linear units on an expanded horizontal scale ($-\pi/16$ to $+\pi/16$). The Fourier transform of this beampattern shows the bandlimited angular frequency cutoff at $\chi = \Gamma/\lambda$.

2.1. Spectrum Restoration

This technique is an iterative method of correcting the distortion produced by the array in estimating the true spectrum. Adjustment ΔM to an initial approximation of the true directional power spectrum M_{app} is accomplished by subtracting the convolved output of M_{app} and the known array beampattern A, from the measured directional power spectrum M_a;

$$\Delta M = M_a - (A * M_{app}).$$

The initial approximation M_{app} is adjusted producing a new approximation for the next iteration, proceeding until the adjustment is small; typically only a few iterations are required. Using the array beamformed output M_a as the initial approximation, the procedure is shown below;

$$M_n = M_{n-1} + (M_a - A * M_{n-1}).$$

The resulting restored spectrum remains band limited because of the angular resolution of the array and is termed the principle solution, restoring the components within the array's measurement capability. If the true spectrum contains components outside the band of the array (>χ in Figure 6), then the Fourier transform of the principle solution will contain a discontinuity at χ which may produce oscillatory characteristics in the restored spectrum. To illustrate the seriousness of this effect for the vertical array measurement of the ambient noise field, a simulated field was constructed (Figure 7). This field is defined in terms of normalized wave number

$$\frac{\psi}{2\pi} = k(\frac{d\sin\theta}{2\pi}),$$

where the limits of visible space correspond to $\sin\theta = \pm 1$, or $-kd \geq \psi \leq +kd$; k is the wave number, d is the array element spacing and θ is the look direction. It is possible to incorporate phase delays which correspond to space that is not physically realizable. This space is referred to as invisible space and the beams corresponding to delays > |kd| are called virtual beams. The ambient noise field used for this simulation is typical of ambient noise at 55 Hz with high angular frequencies (Figure 7a). This field was convolved with a known array beampattern (Figure 7b) at 55 Hz to produce the measured spectrum (Figure 7c) which was introduced as the initial approximation in the iterative restoration scheme. Comparing the principle solution (Figure 7d) to the true spectrum (Figure 7a) illustrates their differences incl .ding: overshoot in regions of sharp angular change, oscillation particularly in the invisible region, a slight broadening of the pedestal width and a small amplitude deviation of less than 0.5 dB. An example of restoration of the ambient noise data discussed in the following sections is shown in Figure 8. The array beampattern (Figure 8a) used a Kaiser-Bessel (α=1.5) amplitude weighting function and the estimated array amplitude and phase calibration errors [Sotirin and Hodgkiss, 1989]. The original angular distribution (recorded on Julian day 270 at 0400 GMT) is typical of ambient noise data at high wind speed for 55 Hz with a 15 dB pedestal approximately between $\pm 18°$ of horizontal. Restoration sharpens the discrete source components, minimally increasing the peaks and decreasing the valleys, but preserves the absolute levels and overall shape. There are noticeable oscillations in this example, particularly at the higher angles. The gain in directional resolution, particularly in the pedestal region, is offset by the additional processing required, the relatively minor level corrections, the obscure distinction between

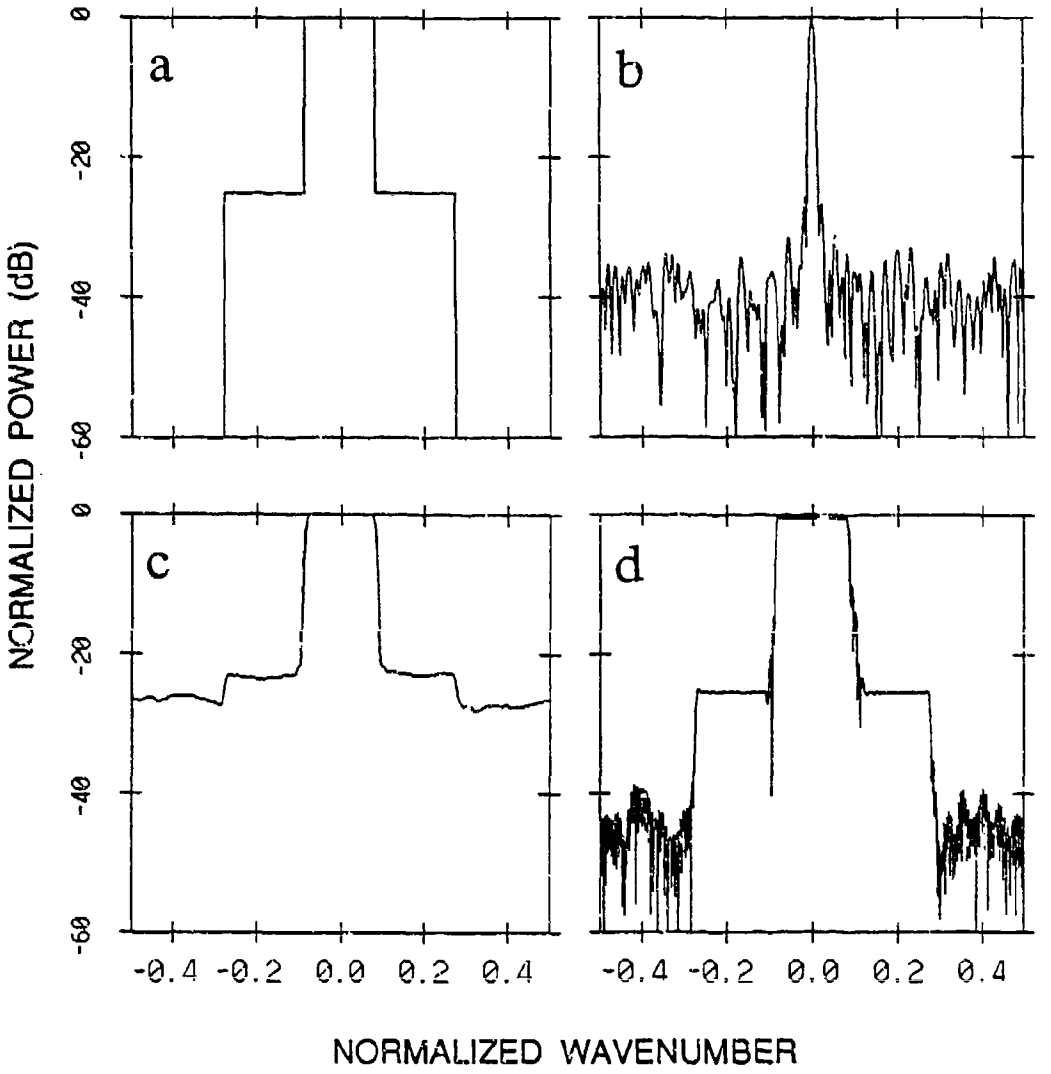

Figure 7 Spectrum restoration simulation. The spectrum restoration method is test for simulated ambient noise data by defining the "true" vertical ambient noise field where the ambient noise pedestal is represented here with a 0 dB level between ±0.085. The level then drops to -25 dB until the limit of real space at ±0.275, beyond is invisible space at a -100 dB level. This "true" noise field (a) is convolved with a known array beampattern at 55 Hz (b) to provide a measured spectrum (c) with which to test the method expecting to restore the original spectrum (a). The resulting solution is shown in (d) to exhibit some oscillatory characteristics and a slight level decrease.

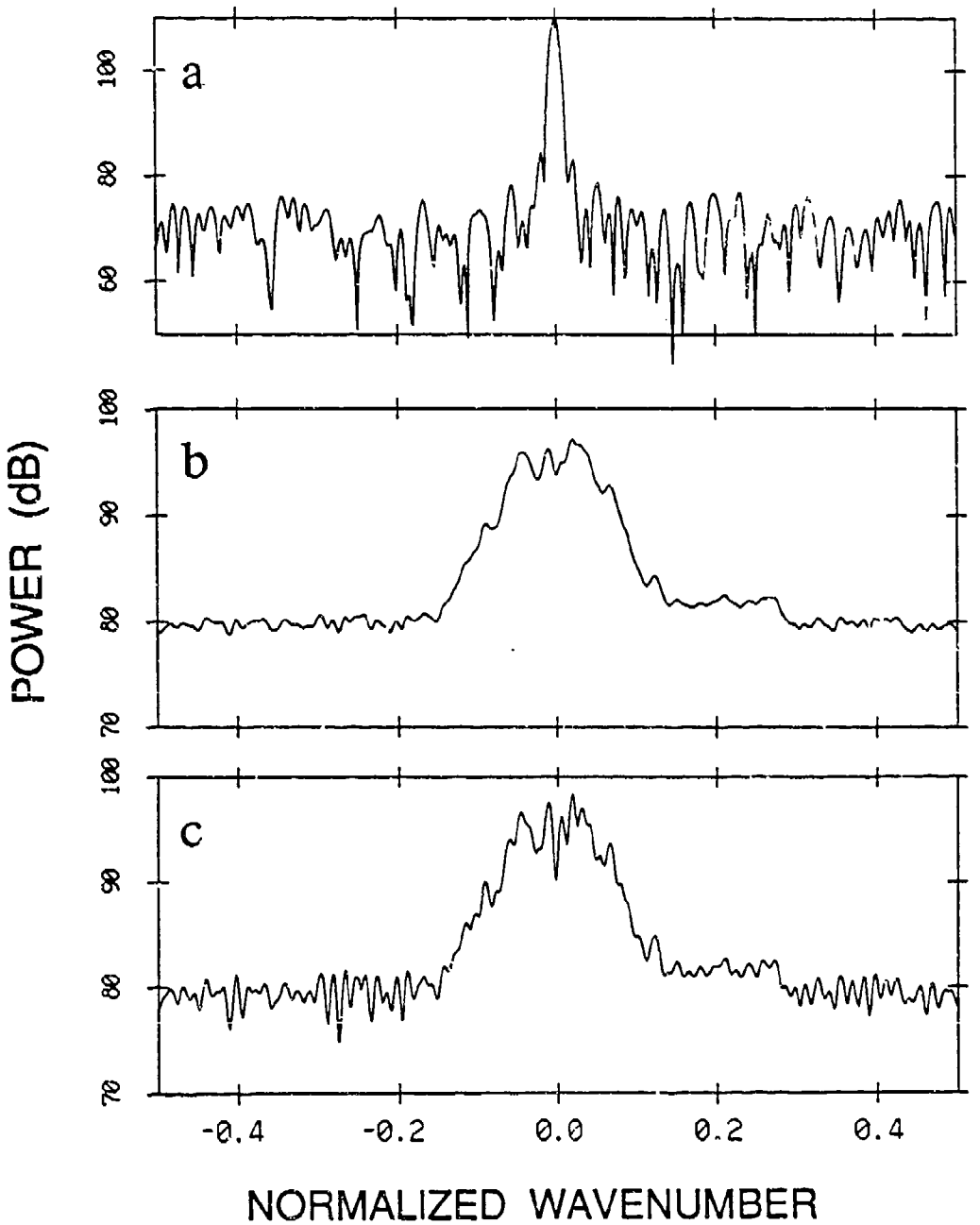

Figure 8 Ambient noise spectrum restoration. A representative example of the spectrum restoration using array beamformed data at 55 Hz from Julian day 270 at 0400 GMT with an 11 m/s wind speed. The positive angles represent upward looking angles. The array beampattern used in the restoration is shown in (a), the original angular spectrum is shown in (b) and the restored spectrum is shown in (c). The restoration increased the peaks in the pedestal by as much as several dB and decreased the valleys similarly. The levels outside the pedestal exhibit oscillatory characteristics, but in general, the absolute levels and overall shape are preserved.

processing artifacts and restored distribution, and possible errors in the estimated beampattern. Therefore, restoration was not applied to the bulk of the data but used as a tool to aid in data interpretation for select cases.

The small differences between the measured noise field and the restored noise field outside the pedestal region in Figure 8, indicate that this region is not contaminated by array sidelobe levels as illustrated by the 2-3 dB level change in Figure 7 for the same region. The susceptibility to array sidelobe contamination of different measured distributions is quantified by simulations below.

2.2. Simulations

Insight into the distortion imposed by the array may be gained by convolving a simulated spatial noise field with the array beampattern, and quantifying the result in terms of a main beam to sidelobe ratio. The spatial ambient noise field is approximately described by a ±15° to ±20° pedestal at a level of 5 to 30 dB above the high angle level where "high angles" are defined to be visible space outside the pedestal region. Although the pedestal height is defined relative to the high angle level, a change in pedestal height actually reflects a change in the high angle level as opposed to a change in the pedestal level. The array beampattern is approximately described by a narrow rectangular main beam with flat sidelobes at -30 to -35 dB. The width of the rectangular main beam is calculated to provide a power gain equivalent with that achieved with the calibrated main beam, shown in Table 1 as equivalent beam width (EBW) for a broadside and 45° looking beam. For the normalized beampattern in Figure 6, the EBW = $\sum_{n=-\frac{\lambda}{\Gamma}}^{+\frac{\lambda}{\Gamma}} B(n\theta)$ where $B(n\theta)$ is normalized power magnitude shown in the figure. The main beam to sidelobe ratio (MSR) is then defined as the integrated power seen by the main beam when it is steered to a specified direction over the integrated power seen by the array sidelobes, given the known spatial ambient noise field.

Frequency (Hz)	15	35	55	75	95	105	115	125
broadside EBW	8.4°	3.6°	2.3°	1.7°	1.3°	1.2°	1.1°	1.0°
45° look angle EBW	12.1°	5.1°	3.3°	2.4°	1.9°	1.7°	1.6°	3.7°

Table 1. Equivalent beamwidth.

Two sets of simulations were conducted. The parameters varied during the simulations were pedestal width, pedestal height, array sidelobe level, look direction and frequency. The first set was conducted at 55 Hz for various spatial noise fields and array sidelobe levels with results shown in Table 2. The noise fields considered were ±15° pedestal width at power levels of 10, 20 and 30 dB above the high angle levels, and ±18 and ±20° widths at 10 and 20 dB levels. Two array sidelobe levels were specified at -30 and -35 dB relative to the main beam, and two look directions were specified at broadside and +45°. Interpretation of

Noise field description	Array sidelobe level (dB)	Mainbeam to Sidelobe Ratio (dB)	Look direction
flat	-30	1.1 1.3	broadside +45°
	-35	1.6 1.8	broadside +45°
±15° pedestal	-30	1.7 0.90	broadside +45°
at 10 dB	-35	2.2 1.4	broadside +45°
±15° pedestal	-30	1.9 0.08	broadside +45°
at 20 dB	-35	2.4 0.57	broadside +45°
±15° pedestal	-30	1.9 -1.0	broadside +45°
at 30 dB	-35	2.4 -0.40	broadside +45°
±18° pedestal	-30	1.7 (0.75) 0.85	broadside +45°
at 10 dB	-35	2.2 1.3	broadside +45°
±18° pedestal	-30	1.8 (4.0) 0.0	broadside +45°
at 20 dB	-35	2.3 (1.75) 0.49	broadside +45°
±20° pedestal	-30	1.7 0.81	broadside +45°
at 10 dB	-35	2.2 1.3	broadside +45°
±20° pedestal	-30	1.8 -0.05	broadside +45°
at 20 dB	-35	2.3 0.43	broadside +45°

Table 2. Mainbeam to sidelobe ratio (dB) at 55 Hz.

the MSR results are enhanced by examing the relative differences in angular component levels. That is, for a pedestal of ±18° width and 20 dB height, the convolved response accurately measures the pedestal width but distorts the height. Relative differences between the true height and the convolved height are shown in parenthesis in Table 2 preceding the corresponding MSR for selected cases. To achieve a measured response to within a 1 dB level of the true distribution requires an MSR of about 0.85 dB. The results show that the MSR is more than adequate to measure the pedestal distribution irrespective of the specific parameters, however the higher angle levels are sometimes distorted. As the pedestal width is increased, the MSR decreases as more energy is picked up by the array sidelobes. As the pedestal height is increased, the MSR at the +45° look angle decreases. The second set of simulations was conducted for various frequencies, pedestal heights of 10 and 20 dB and a constant pedestal width of ±18°, which approximates the ambient noise field observed during the experiment. The results, shown in Table 3, exhibit a decreasing MSR with increasing frequency, expected as the main beam width decreases.

Frequency (Hz)	Noise field description		Mainbeam to Sidelobe Ratio (dB)	Look direction
15	±18° pedestal	10 dB	2.8 2.0	broadside +45°
		20 dB	3.0 1.2	broadside +45°
35	±18° pedestal	10 dB	2.4 1.6	broadside +45°
		20 dB	2.5 0.69	broadside +45°
55	±18° pedestal	10 dB	2.2 1.4	broadside +45°
		20 dB	2.3 0.49	broadside +45°
75	±18° pedestal	10 dB	2.0 1.2	broadside +45°
		20 dB	2.2 0.34	broadside +45°
95	±18° pedestal	10 dB	1.9 1.1	broadside +45°
		20 dB	2.1 0.2	broadside +45°
115	±18° pedestal	10 dB	1.9 1.0	broadside +45°
		20 dB	2.0 0.15	broadside +45°

Table 3. Mainlobe to sidelobe ratio (dB) with -35 dB array sidelobes.

It has been suggested that virtual beam levels (beams outside visible space) may be used to indicate the sidelobe suppression levels of an array [Berrou,

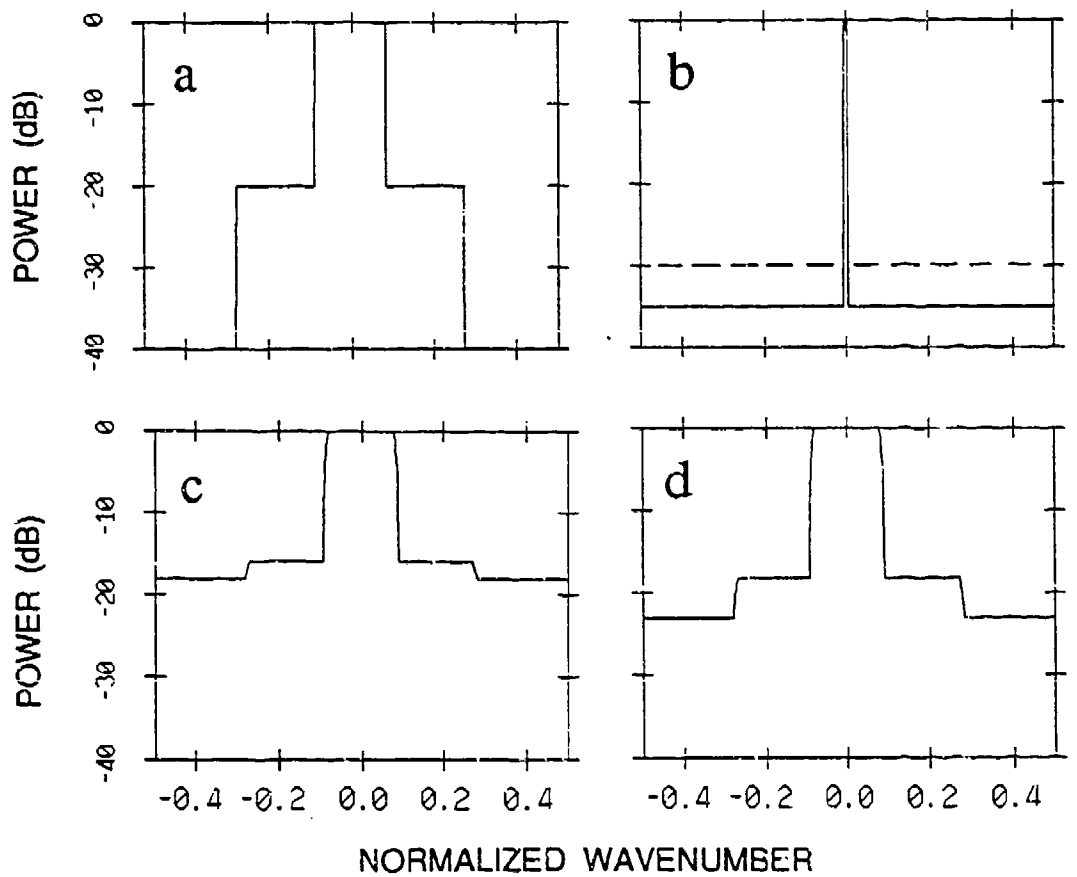

Figure 9 Virtual beam simulation. Virtual beams are those whose phase delay does not correspond to a part of the visible spectrum. At 55 Hz, these beams are those between +0.275 to +0.5 and -0.275 to -0.5. The drop in level between real space and invisible space is a function of the ambient noise field and the array characteristics. The original spectrum (a) is convolved with the array beampattern (b) shown for two sidelobe levels. The simulation results (c) and (d) represent sidelobe levels of -30 dB and -35 dB respectively.

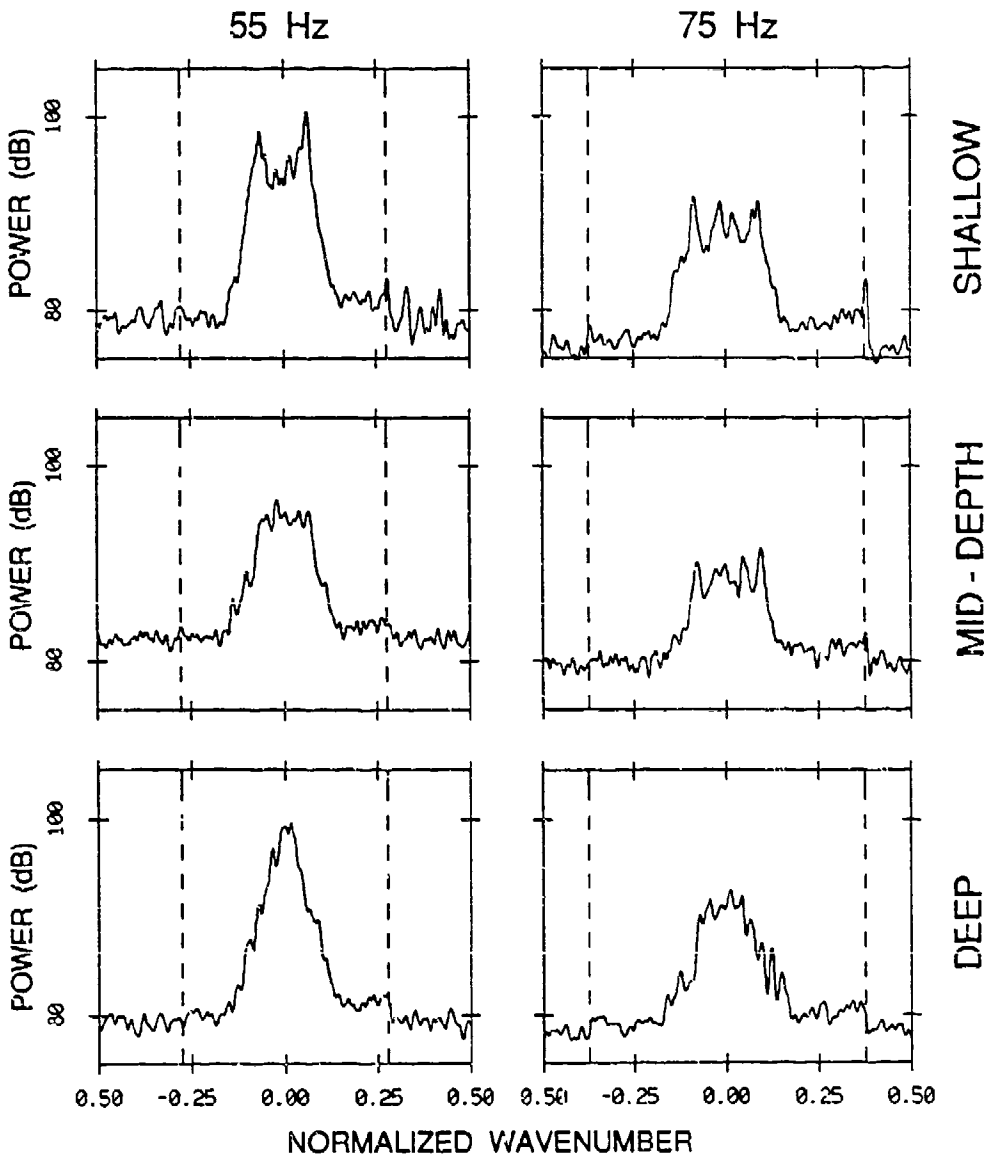

Figure 10 Measured virtual beam levels. The drop in level between real space and invisible space for vertical ambient noise is seen at 2 to 5 dB levels. The data were recorded during relatively high wind conditions (11.3 m/s) at three array depths.

Bluy and Wagstaff, 1982; Wagstaff, 1988]. The virtual beam level is indeed a function of the array sidelobe level however other significant factors (array main beam width, directional spectrum input) affect this level such that its interpretation is not straight forward. For the directional spectrum provided by a typical ambient noise field, and the specific characteristics of the array considered here at 55 Hz, the drop in level between visible beams and virtual beams is shown in Figure 9 to be less than 5 dB for array sidelobe levels of -35 dB and about 2 dB for sidelobe levels of -30 dB. If the array calibration errors were to be included in the array beampattern, the drop would be even less conspicuous. For a wider main beam and a strong directional source [Wagstaff, Berrou and Cotaras, 1982], this technique may be more valuable as an array assessment tool. The directional spectrum in Figure 9 is plotted in terms of normalized wavenumber where ± 0.275 represent the limits of visible space. The 'real' data represents a $\pm 18°$ pedestal width at a 20 dB level relative to the higher angles and 100 dB relative to the invisible space level. The -100 dB level of the virtual beams represents the array electronic noise floor, mechanical energy, and energy from incoherent sources. The array sidelobe levels were constant at -30 and -35 dB relative to the main beam. The virtual beam level is demonstrated for experimental measurements in Figure 10 where the expected drop is evident particularly for 75 Hz whose corresponding MSR is less that that at 55 Hz.

The beamformed array data reflects the true ambient noise directional spectrum with some constraints. The beamformer has been shown to have limitations in wave number and vertical arrival angle resolution due to discrete sampling and a nonzero main beamwidth. The large number of elements in this particular array minimizes the distortion caused by the beamwidth but increases concern regarding array sidelobe levels. By observing the main beam to sidelobe ratio under various noise field conditions, it is seen that the array correctly estimates the level and width of the ambient noise pedestal but distorts the high angle level. This amount of distortion increases with frequency, pedestal height and pedestal width. For a $\pm 18°$ pedestal, the array is capable of measuring a 10 dB pedestal height to within 1 dB at all frequencies considered, however as pedestal height increases to 20 dB, the MSR decreases with frequency until at 115 Hz, there is approximately a 3 dB error in high angle level.

3. VERTICAL DIRECTIONALITY AS A FUNCTION OF WIND SPEED

The large array aperture (900 m) provides greater directional resolution than any previous work at low frequency. While increasing the resolution, the large aperture also raises concerns about the validity of conventional beamforming due to array shape and wavefront curvature. The array was equipped with an acoustic navigation system [Sotirin and Hildebrand, 1989] which, for the data set presented here, showed the array was straight and vertical to within 1°. Wavefront curvature, resulting from variations in sound speed across the array aperture, is not a major source of error in the ambient noise analysis [Tran and Hodgkiss, 1989], mainly affecting signals arriving within $\pm 5°$ of horizontal with small losses in signal level and a slight distortion in arrival angle. Another concern is mechanical motion or array strum injecting signals which could interfere with ambient noise measurements. It is shown below that although the array does exhibit strum characteristics, the signals are narrow in frequency and in apparent direction.

Ambient noise directionality data were studied at various array depths and local wind speeds. During the passage of a storm, the array was deployed at

three depths, provides an opportunity to examine the variation with depth at three nominal wind speeds. Nine 2-minute data segments were processed. The mid-array depth for the three deployments were 850, 1750 and 2650 m, and recorded wind speeds were within 0.5 m/s of 3.1, 7.2 and 11.3 m/s, for the low, medium and high designations. The passage of another storm increased local wind speed from 2 to 12 m/s over a 21 hour period. Two minute samples were selected every 20 minutes during this event to provide a detailed investigation of the directional variability with increasing wind speed.

3.1. Data Processing

Data integrity was verified by examining time series and spectra for representative elements. Two-second time series of the 120 channels were scanned at the beginning, middle and end of the 21 hour time series to note any channel variations during the storm. For each 2 minute segment analyzed, the time series for a representative element was plotted over the entire segment to identify any obvious contaminants, such as a seismic profiler operating off the California coast. The profiler signature was perceptible in the time series as shown in Figure 11, and was removed prior to subsequent processing. Calculating the spectra of one channel per array section provided a mid-process verification of the data.

Further processing consisted of selecting desired frequency bins, compensating for an array sampling offset [Sotirin and Hodgkiss, 1989] and beamforming across the full array aperture as well as two 20 element subsections. The data segment (65536 samples for each of the 120 channels) was frequency transformed using a 1024-point Fast Fourier Transform (FFT) after application of a Kaiser-Bessel (α=2.5) window. Spectral estimates (0.49 Hz/bin) were selected at 5 Hz increments from 15 to 130 Hz, avoiding narrow band contaminants at 60, 115 and 120 Hz by shifting to 61.0, 113.8 and 118.7 Hz. A frequency dependent phase correction was implemented to account for the sampling offset. The spatial conversion was accomplished using an FFT beamformer, analogous to the time to frequency domain FFT as discussed below for the simple example of a single narrowband plane wave arrival. For a time sampled plane wave signal $s(t) = e^{j\omega t}$ arriving at the array at an angle θ from the horizontal, the output of the nth array element is $a_n(t) = s(t + \frac{nd\sin\theta}{c})$ where d is the array element spacing, and c is the propagation speed. A time delay beamformer is a delayed sum of the N weighted element outputs; for the m^{th} beam B_m and weights w_n:

$$B_m = \sum_{n=0}^{N-1} w_n\, a_n(t-\tau_{n,m}) = \sum_{n=0}^{N-1} w_n s(t + \frac{nd\sin\theta}{c} - \tau_{n,m})$$

$$= \sum_{n=0}^{N-1} w_n e^{j\omega t} e^{j\omega\frac{nd\sin\theta}{c}} e^{-j\omega\tau_{n,m}}$$

where the time delay for the nth element corresponding to the beam B_m with look direction θ_m, is $\tau_{n,m} = n\,\frac{d\sin\theta_m}{c}$. Since $c = f\lambda$, then $\frac{\omega}{c} = \frac{2\pi}{\lambda}$ which is defined as the wavenumber k. Substituting,

$$B_m = \sum_{n=0}^{N-1} w_n e^{j\omega t} e^{-j(nkd\sin\theta_m - nkd\sin\theta)} = \sum_{n=0}^{N-1} A_n e^{-jnkd\sin\theta_m}$$

where $A_n = w_n e^{j\omega(t + \frac{nd\sin\theta}{c})} = w_n e^{j(\omega t + nkd\sin\theta)}$ represents the weighted response of the nth element induced by the signal s(t). Defining ϕ_m as $kd(\sin\theta_m)$, this specialized result may be evaluated using FFT algorithms:

$$B_m = \sum_{n=0}^{N-1} A_n e^{-jn\phi_m}.$$

In general, the noise field arriving at the array would be broadband in frequency and arrival angle and the FFT beamformer is implemented as:

$$B_{l,m} = \sum_{n=0}^{N-1} A_{l,n} e^{-jn\phi_{l,m}}$$

where $A_{l,n}$ is the complex one-sided frequency domain FFT output of the received signal at the lth frequency and the nth element, and $B_{l,m}$ is the spatial domain FFT output for the lth frequency and the mth beam. The beamformer was specified with M=512 points, a Kaiser-Bessel (α=1.5) shading function w_n and a spatial sampling frequency of 0.131579 samples/meter. This sampling deviates slightly from the array design element spacing of 7.5 m due to strain in the kevlar strength member under tension. The parameters of the temporal transform are compared to the spatial transform in Table 4 to clarify the spatial spectrum normalization discussed below. The spatial samples were incoherently averaged, and converted from electrical angle ϕ to physical angle $\theta = arcsin(\phi/kd)$. The average magnitude-squared results were calibrated to dB re 1 μPa/$\sqrt{Hz}$ Deg by normalizing by the number of points N, the power in the window function ($\frac{1}{N}\sum_{n=0}^{N} w_n^2$) and the spatial sampling frequency, and by converting wavenumber to degrees with the factor

$$dk_\nu/d\theta = \frac{\pi f}{180c}\cos(\frac{\pi}{180}\theta)$$

where k_ν is the digital spatial frequency $\frac{1}{\lambda}\sin\theta$ analogous to the digital time frequency f. This normalization presents the data in terms of average narrowband intensity received by the array per vertical degree.

3.2. Array Strum

The mechanical vibrations of the array, induced by water currents and surface platform motions, are limited to low frequencies (5-30 Hz). There are two modes of vibration identified in the array time series data which may potentially contaminate the ambient noise data. The transverse component, modeled as if the array were an infinitely flexible string, has a computed speed of $c = \sqrt{T/\mu}$ where T is the tension (Newtons), and μ is the array mass/unit length (kg/m), and assuming standing wave propagation, the frequency is $\nu_n = nc/2\Gamma$, where n=1 for the fundamental frequency, and Γ is the length of the string [Morse and Ingard, 1968]. The array system is composed of 4 component parts: uplink wire, array, kevlar strength member and weights. The system mechanical parameters were estimated as follows: mass of 1887 kg, center of mass at 954 m, weight in water of 5880 N

Temporal	Spatial	Mode
$\omega_c = \frac{2\pi}{T} = 2\pi f$ f = temporal frequency	$k_c = \frac{2\pi}{\lambda}$ $\frac{1}{\lambda}$ = spatial frequency	continuous
$\omega_d = \omega_c T_s = \frac{2\pi f}{f_s}$ f = temporal frequency f_s = temporal sampling frequency	$k_d = \frac{2\pi}{\lambda} d\sin\theta$ $\frac{\sin\theta}{\lambda}$ = spatial frequency $\frac{1}{d}$ = spatial sampling frequency	discrete

Table 4. Temporal vs. spatial transform parameters.

and density of 1.44 gm/cm^3. Using these parameters for an infinitely flexible string with uniformly distributed mass and small displacements, the velocity of a transverse wave traveling down the array would be 54 m/s, and the fundamental frequency assuming standing waves would be about 0.03 Hz. Velocity measurements of this component are difficult because of the relatively low amplitudes and propagation interference due to the stiff section splices and processor pressure cases, however, from a typical time series plot [Sotirin and Hildebrand, 1988, Figure 8] the speed is estimated to be 43 - 53 m/s, comparing favorably to the calculated speed. The speed and frequencies characteristic of the longitudinal mode are more difficult to predict because of uncertainty in elastic moduli estimation. Observationally, the longitudinal mode is more apparent than the transverse mode, traveling down the array at a measured speed of 1800 m/s from the surface and a frequency of about 20 Hz. Since the speed of propagation for ambient noise beamforming is 1500 m/s, signals propagating at other phase velocities appear at non-endfire angles. Using Snell's law:

$$\frac{c_1}{\sin\theta_1} = \frac{c_2}{\sin\theta_2}$$

where c_1 = 1800 m/s, c_2 = 1500 m/s, and θ_1 = 90°, gives θ_2 = 56°. A series of directional spectra with prominent longitudinal strum are shown in Figure 11 demonstrating the arrival structure and time variability of the strum events.

The transverse component of strum is not apparent in the directional measurements due to its low amplitudes and relatively slow propagation speed. The longitudinal mode however, is evident in the ambient noise directional spectrum at arrival angles from 45° to 65°. The angular isolation of the strum signal allows the pedestal structure of the ambient noise field to be analyzed without contamination unless the strum signal is strong enough to compete with the power seen by the mainbeam through array sidelobe leakage.

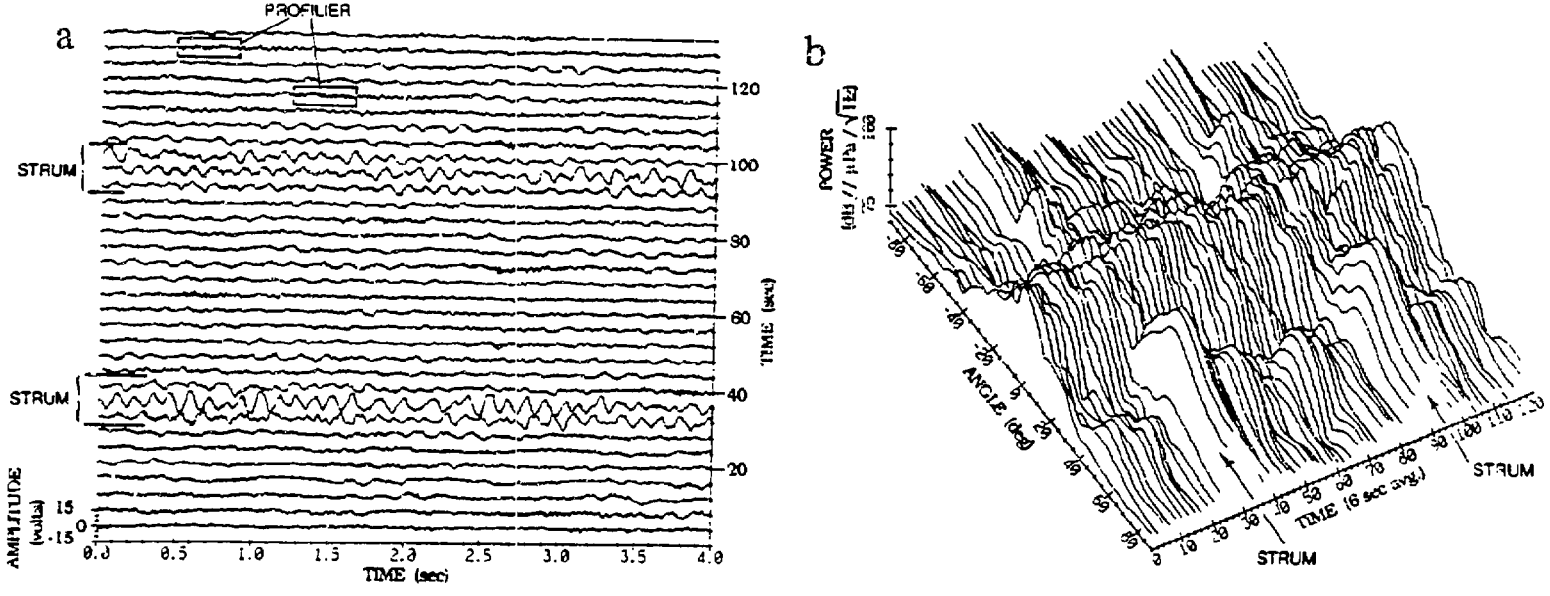

Figure 11 Array strum arrivals. The time series (a) of one element in the array over 2 minutes shows strong mechanical vibration events which travel down the array from the surface with an attenuated reflection at the bottom. A running directional spectrum (b) consisting of 6 second averages and 2 second shifts between estimates shows the apparent directional structure of the strum signal as a broad arrival centered at about 56°. The zero-crossing main beamwidth at 20 Hz and a 56° look angle is 35°.

3.3. Ambient Noise as a Function of Wind Speed

Ambient noise has been shown to be a function of frequency, location, depth, direction and source mechanism. The frequency dependence of ambient noise has been studied extensively and is summarized by Urick [1984]. We consider the frequency band between 15 and 130 Hz, referred to in the literature as the low frequency band or low sonic band (20-200 Hz). Within this band the predominant sources are man-made (shipping and seismic exploration) and environmental (wind and wave induced turbulence). The importance of location is related to the proximity of major shipping lanes and storm tracks. The difference in spectral levels with depth is small until critical depth (where the sound speed at depth is equal to that at the surface) is reached [Morris, 1978]. Directional characteristics, the major emphasis of the data analysis below, is far from isotropic, depending on source distribution and relative strength, and propagation parameters such as sound speed profile, mid-water reverberation and range dependent boundary coefficients. The purpose of this report is to investigate the influence of local storms on the directional spectra of low frequency ambient noise data collected in the NE Pacific above the critical depth.

Low frequency measurements show persistent directional characteristics, associated with distant shipping lanes and density patterns, which are smoothed by environmental contributions. This dependence is manifested in vertical distributions as a broad, angular distribution of noise intensity near the horizontal referred to as the ambient noise pedestal. The range of angles spanned by the pedestal, or pedestal width, is a function of the ocean boundary and refractive effects on propagation. Pedestal height refers to a relative measure, and reflects the contributions from shipping and environmental sources arriving at near horizontal angles relative to those arriving at higher vertical angles, whereas absolute pedestal level refers to the average absolute level of the pedestal. Coastal shipping, narrow in frequency and direction, and coastal storms, which fill in the spectrum, may be converted to horizontal angles by downslope conversion [Wagstaff, 1981]. Other distant shipping noise may be converted to horizontal angles by surface reflecting rays which refract at a depth above the ocean floor. High latitude storms may also contribute by means of the depth varying sound speed minimum [Anderson, 1979; Bannister, 1986]. Outside the pedestal, local effects may dominate. The patterns which reflect distant sources are confined to low frequencies and near horizontal angles due to the relatively low attenuation for non-bottom interacting paths.

The data discussed here were recorded during September 1987 in a high shipping density area about 400 nm west of Monterrey, CA in deep (4667 m) water. Spectral levels are consistent with high shipping density [Urick, 1984] when the effects of the seismic profiler operating off the California coast are removed; measurements at 100 Hz were about 79 dB re μPa/$\sqrt{\text{Hz}}$ for low wind speeds. The absolute pedestal level at 100 Hz were about 62 dB re μPa/$\sqrt{\text{Hz}}$ Deg. These levels are slightly higher (2 dB) than those measured by Hodgkiss and Fisher [1987], and we observed a pedestal height at low wind speeds about 10 to 15 dB lower. For a typical measurement of 12 dB pedestal height over $\pm 16°$, the power integrated over the pedestal is 3.5 times that contained in the higher angles. Thus, omnidirectional spectral levels would only deviate on the order of 1 dB due to the power difference in the higher angles. Estimating levels from gray-level type plots, it would appear that the pedestal height for data at 100 Hz measured at 30° from broadside, shown by Carey, *et al* [1985] is 12-13 dB, whereas Wales and Diachok [1981] measured about 10 dB. Burgess and Kewley [1985] present data measured in the South Fiji basin, where ship traffic is light, having lower absolute

levels and a 15 to 20 dB pedestal height. Since broadside levels are a function of the proximity of shipping lanes and storm tracks, a lower absolute level is expected.

The test site 400 nm off the coast of California was affected by major shipping lanes to the north, coastal shipping to the east and for the duration of the experiment, storm tracks to the south, an area riddled with complex bottom topography providing opportunities for downslope conversion [Morris, 1975]. Using only a vertical array, however, the azimuth of the pedestal source is not determinable.

Although ambient noise is normally considered to exclude identifiable ship sources, with increased directional resolution, the effect of ships (identified as angular point sources) at times dominates the pedestal structure. Arrays with less resolution smear these arrivals, producing a much smoother distribution. To allow comparison, the discrete sources should be integrated. To measure the true value of ambient noise an estimate of the level between the discrete ship sources should be recorded (thereby smoothing over signals which are not resolved by the present array). At 100 Hz, the inter-ship level in the pedestal is about 57 dB re μPa/$\sqrt{\text{Hz}}$Deg for wind speeds up to 10 m/s, this level increased by several dB at about 1500 GMT, possibly due to downslope conversion of energy from the approaching storm.

Surface ships at propagation convergence zones also present strong directional lines which can vary rapidly with time (Figure 12), the magnitude changing as much as 2.5 dB/minute. A limited radar range was available during the experiment, so ships further away than 42 km (just short of the first convergence zone) were not logged. The strong narrow beam signals outside the pedestal are most probably generated by the same ship at fairly close range even though it was not observed by radar. A surface source at a range of 27 km would arrive at the array with one bottom bounce at +24° and two bottom bounces at -31° and +38° as seen in Figure 12.

Ray diagrams are helpful in visualizing pedestal dynamics. Ambient noise pedestal height reflects the energy trapped in the deep sound channel and pedestal angular width is defined by the bottom grazing rays (Figure 13a). The structure of the pedestal is modified by rays which reflect from the surface and whose turning depth is above the ocean floor such that the energy is not attenuated by bottom interaction. These rays transfer surface noise to the array increasing the pedestal height within a narrow band of angles, thereby producing the pedestal "ears" exhibited at certain times. The distribution varies slightly with array depth and with local environmental conditions which are discussed below.

During the passage of a storm where wind speed increased from 2 to 13 m/s, the array depth was varied such that elements spanned the water column from 400 to 3100 m, albeit at different times. The mid-array depths were 850 m, 1350 m and 2650 m. The differences, as a function of these depths, in the directional spectrum are expected to be small, with the pedestal width decreasing slightly [Anderson, 1979]. The range of angles which exhibit the pedestal characteristics and surface shipping "ears" vary with array depth as shown in Figure 13a, b and c, however the difference is limited to a few degrees for the range of depths considered here. The pedestal width should decrease slightly from ±15° at the shallow array depth to ±11° at the deep depth, and those arrival angles containing surface noise from reflecting rays should broaden from ±12° to ±15° at the shallow depth to ±6° to ±11° at the deep depth. The amount of surface noise is highly dependent on the amount of ship traffic and its distribution and produces large

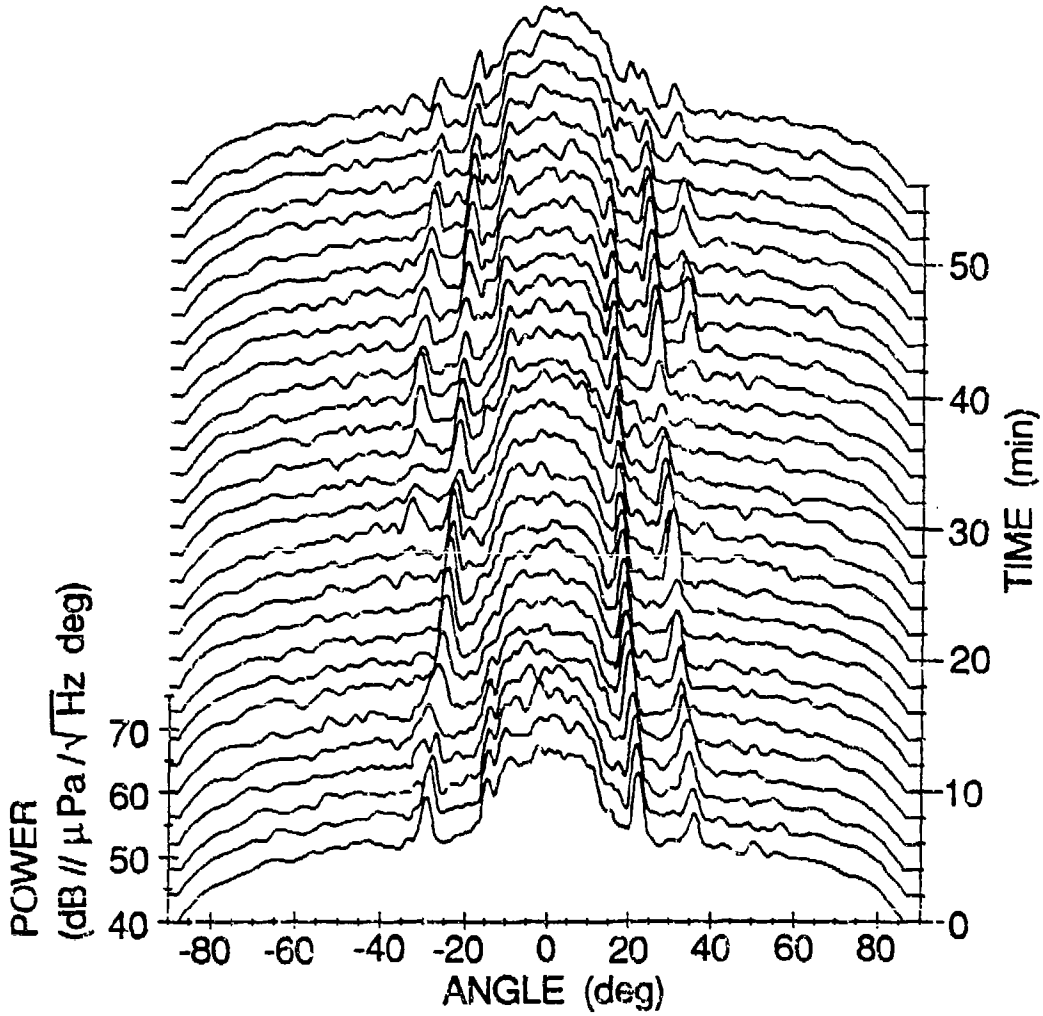

Figure 12 Continuous directional time series. Directional spectral levels were estimated from consecutive 2 minute time segments over 58 minutes at 75 Hz (0.5 Hz bin width). The time samples were recorded on Julian day 268 at 1000 GMT with a mid-array depth of 2650 m and 3 m/s wind speed. The narrow band estimates were shaded with a Kaiser-Bessel (α=1.5) window prior to the spatial transform. The magnitude variation of the signal seen beginning at 38° was as much as 2.5 dB/minute.

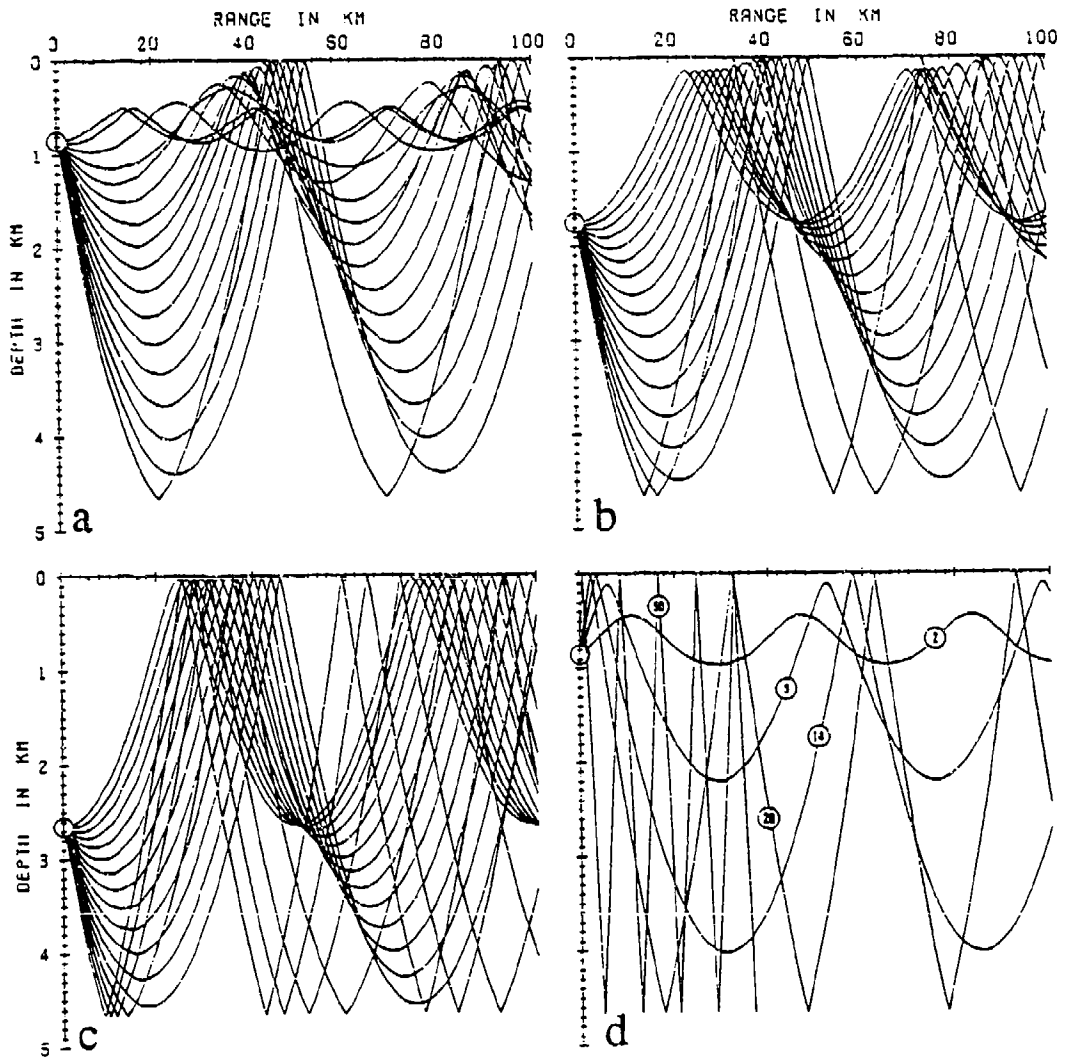

Figure 13 Pedestal rays. The rays producing the ambient noise pedestal vary slightly with array depth for the sound speed profile measured at the experiment site. For the shallow array depth (850 m) (a), the arrival angles contained within the pedestal are between ±15°, and surface noise arrives between ±12° and ±15°. The mid depth (1750 m) (b) pedestal is defined between ±14° with surface noise arriving between ±10° to ±14°. The deep depth (2650 m) (c) pedestal is between ±11° with surface noise arriving between ±6° to ±11°. The ray paths of specific arrival angles are shown (d) which correspond to data in Figure 19. The associated arrival angles are notated.

variations in the measured levels. The pedestal height, since it is relative to the high angle level, is also dependent on wind speed, decreasing as wind speed increases. In general, the measured directional spectrum followed the expected pattern but due to the temporal variability of ambient noise, strong discrete sources and small predicted changes, the observed difference is not significant for the range of depths considered. These predictions are based on the sound speed profile at the experiment site and do not account for the range dependency of the profile. The directional spectrum is shown in Figure 14 at 75 Hz for the three nominal array depths and three wind speeds detailed in Table 5.

Julian Day	GMT	Wind Speed	Array Depth	Tape
266	15:10	low	shallow	688
265	18:02	medium	shallow	634
270	20:25	high	shallow	914
267	13:16	low	mid	736
265	08:38	medium	mid	612
270	03:56	high	mid	878
267	03:28	low	deep	714
268	23:33	medium	deep	812
269	14:04	high	deep	849

Table 5. Vertical Directionality Data: Wind Speed vs. Depth.

The pedestal height tends to decrease with wind speed, and surface noise arrival angle ("ears") decrease with depth, however the predicted decrease in pedestal width is obscured. The array remained above critical depth, where other data have shown substantial decreases [Morris, 1978], so it is not surprising that no significant differences in omnidirectional spectral levels were observed for this range of depths.

The frequency dependent aspects observed in the measured directional spectra are a combination of effects such as frequency dependent attenuation and main beamwidth variability. The increasing beam width of the broadside beam from 2.0° at 95 Hz to 5.5° at 35 Hz (measured at the zero crossings) tends to smooth the spectra as the frequency decreases (Figure 15). The smoothing increases the apparent width and height of the pedestal as narrow beam signals are integrated over adjacent angles. The increase in pedestal height is also due to the decrease in attenuation with decreasing frequency. There is also a slight increase in the levels outside the pedestal at higher frequency about 2 dB between 35 Hz and 95 Hz as seen in Figure 15. The time axis in this figure also corresponds to increasing wind speed as described in detail below. There is a decrease in the pedestal height relative to the high angle level as wind speed increases, and the sharp drop off occurring at 14-15° is obscured as the high angle levels increase. The effect is more apparent in the upward looking angles which at high wind speeds, have slightly more power than the corresponding downward angles. This occurs because the downward looking angles receive the local surface noise via a bottom reflection. Although this difference is small, it occurs at

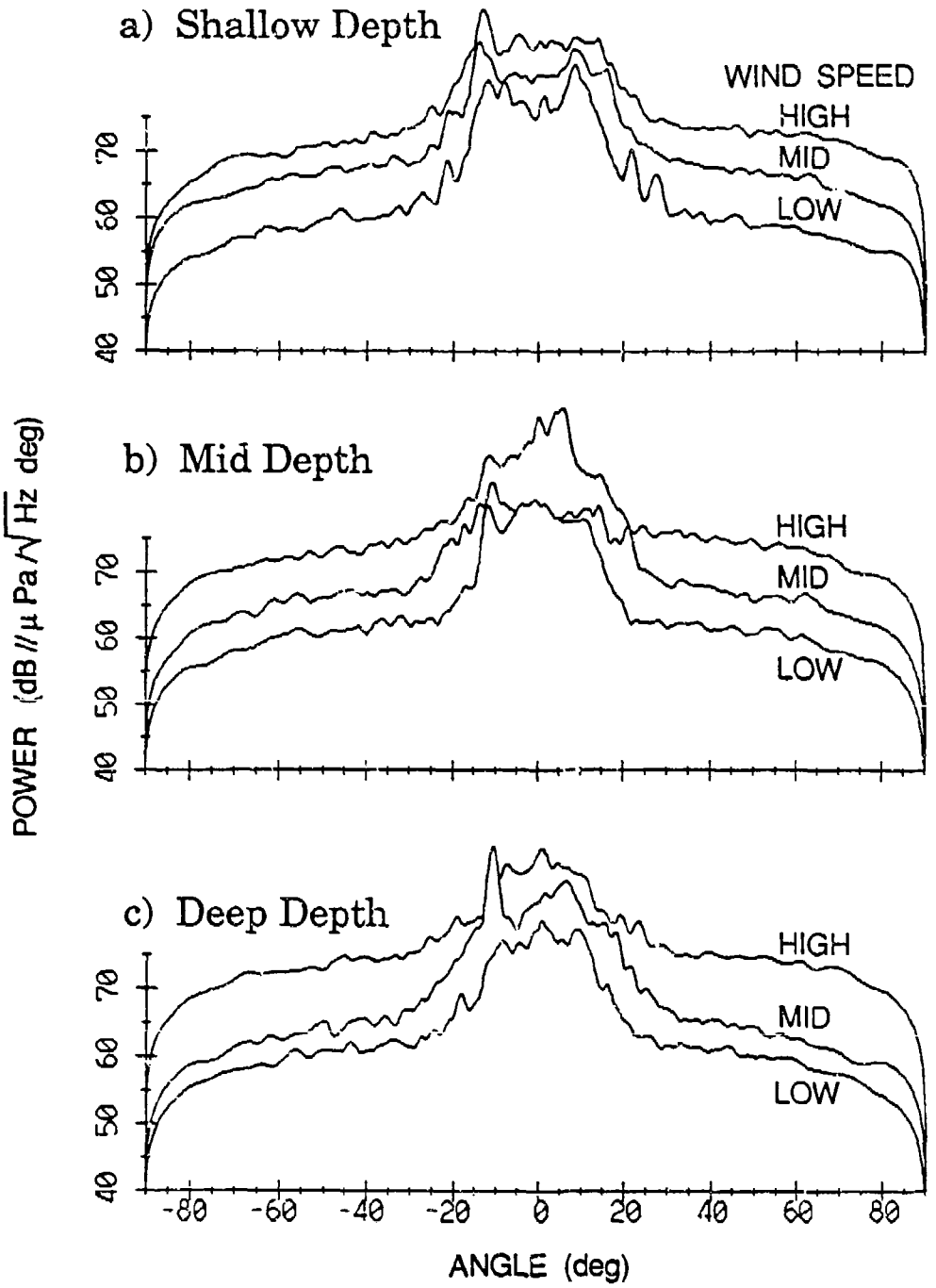

Figure 14 Spatial distribution of ambient noise as a function of depth. The factors impacting spatial distribution with depth are due to the small variation in arrival angles of the rays which define the pedestal shape. In general, the pedestal width should decrease with depth and the "ears" should arrive at angles which are slightly more horizontal. Due to the temporal variability in ambient noise and the strong discrete sources, these effects are not a significant factor for the range of depths considered here. Specific parameters for the data plotted are found in Table 4.5.

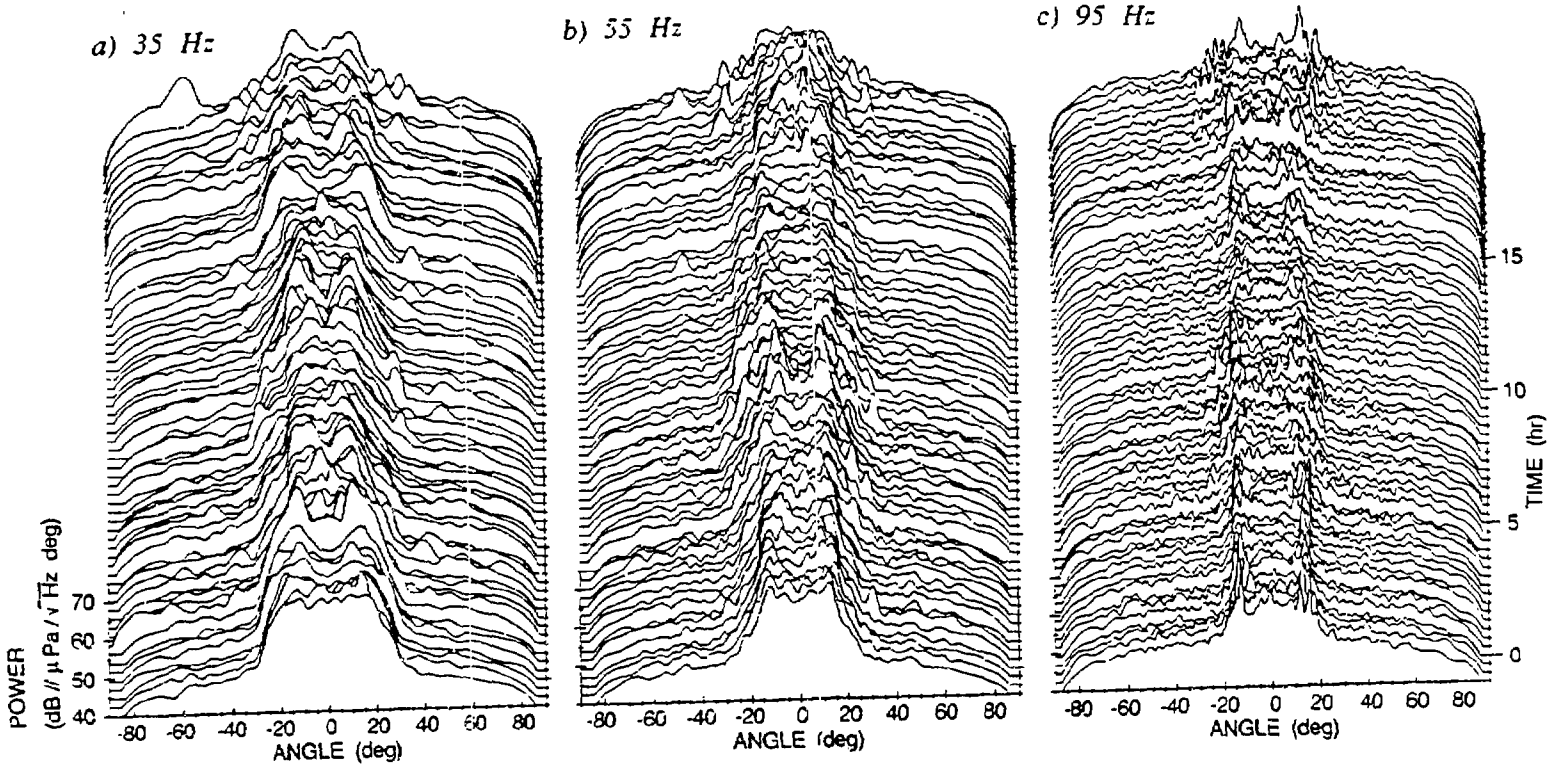

Figure 15 Spatial distribution of ambient noise as a function of frequency. The directionality of ambient noise spectra is shown at 3 frequencies as a function of direction, time and power. The narrowband components (0.5 Hz bin width) are at (a) 35 Hz, (b) 55 Hz and (c) 75 Hz. The time axis also corresponds to increasing wind speed from 2 m/s to 12 m/s. The mid-array depth was at 850 m.

all frequencies, and is measured from Figure 14 to be about 1 dB at 40° and about 2 dB at 70°. The clouding of the pedestal shape is more obvious in Figure 16 which presents data at a low (a) and high (b) wind speed as a function of frequency, angle and power. Absolute pedestal levels are approximately the same for all frequencies above 25 Hz however the increase in the angles outside those defined by the pedestal at high wind speed tends to obscure the pedestal shape. This increase is estimated at 3 to 4 dB and does not appear to be a function of frequency.

The small scale effects of wind speed dependence on ambient noise are more easily observed from deviations about the mean levels. For this particular data set, the wind velocity and swell height were recorded once an hour. The data set analyzed commenced at the onset of an increase in local winds due to the approach (>700 nm) of a hurricane shown on area weather maps. Comparing average array spectral deviations to wind speed estimates in Figure 17, two discrete level changes are observed, one occurring at approximately 1000 GMT and the other at 1420 GMT. The increase in wind speed at 1000 GMT was caused by a squall accompanied by gusting winds and heavy rain but lasting for only about an hour. The corresponding decrease in spectral levels however, is shown not to reflect local conditions but rather distant variations, by the directional spectrum estimates of the same data set discussed below. The individual frequency data (Figure 15) do show a slight increase in the high angle level at 0920 GMT with heavy rain recorded at the local experiment site at 0916 GMT. The second level change is caused by local events, most likely the commencement of breaking waves as the storm intensity increased. Unfortunately estimates of sea state, wave action, or whitecap coverage are not available therefore it is not possible to ascertain absolute source identification and levels. Earlier investigations have interpreted the wind dependent portion of the low frequency spectrum in terms of the logarithm of the wind speed as proposed by Crouch and Burt [1972]; $NL_f = B_f + 20 n_f \log v$ where NL_f is the noise spectrum level in dB re μPa at frequency f, B_f is the spectrum level at a wind speed of 1 knot, n_f is a coefficient determined empirically from the data, and v is the wind speed in knots. The unexplained discrepancy in spectrum level predicted by the coefficients estimated by different investigations was noted by Urick [1984] and tabulated for low frequency by Carey [1987]. The plot of spectral levels vs. linear wind speed (Figure 18) is shown in Figure 18 where the wind dependent portion of the data could be described as those levels above 8 m/s, with spectral levels below 8 m/s dominated by distant shipping or storm noise. Any quantitative relationship to wind speed must account for the relatively sparse and instantaneous estimates of wind speed. Although this data might be interpreted similarly (as a logarithmic dependence), the directional spectrum leads to a slightly different conclusion.

Analysis of the local wind effects is separable from distant changes by observing the directional spectrum deviations. The directional spectrum levels as a function of time are shown at 55 Hz in Figure 15b. Carefully scrutinized, this data shows a decrease in relative pedestal height as time and wind speed increase. By selecting specific directions, the small scale variability is evaluated. These directional data are displayed in Figure 19 for which 4 of the beams point more toward the horizontal and are influenced by distant sources, and 4 of the beams reflect local sources, pointing toward the higher vertical angles. The beams at 50° and 80° are plotted with the corresponding downward looking beams at -50° and

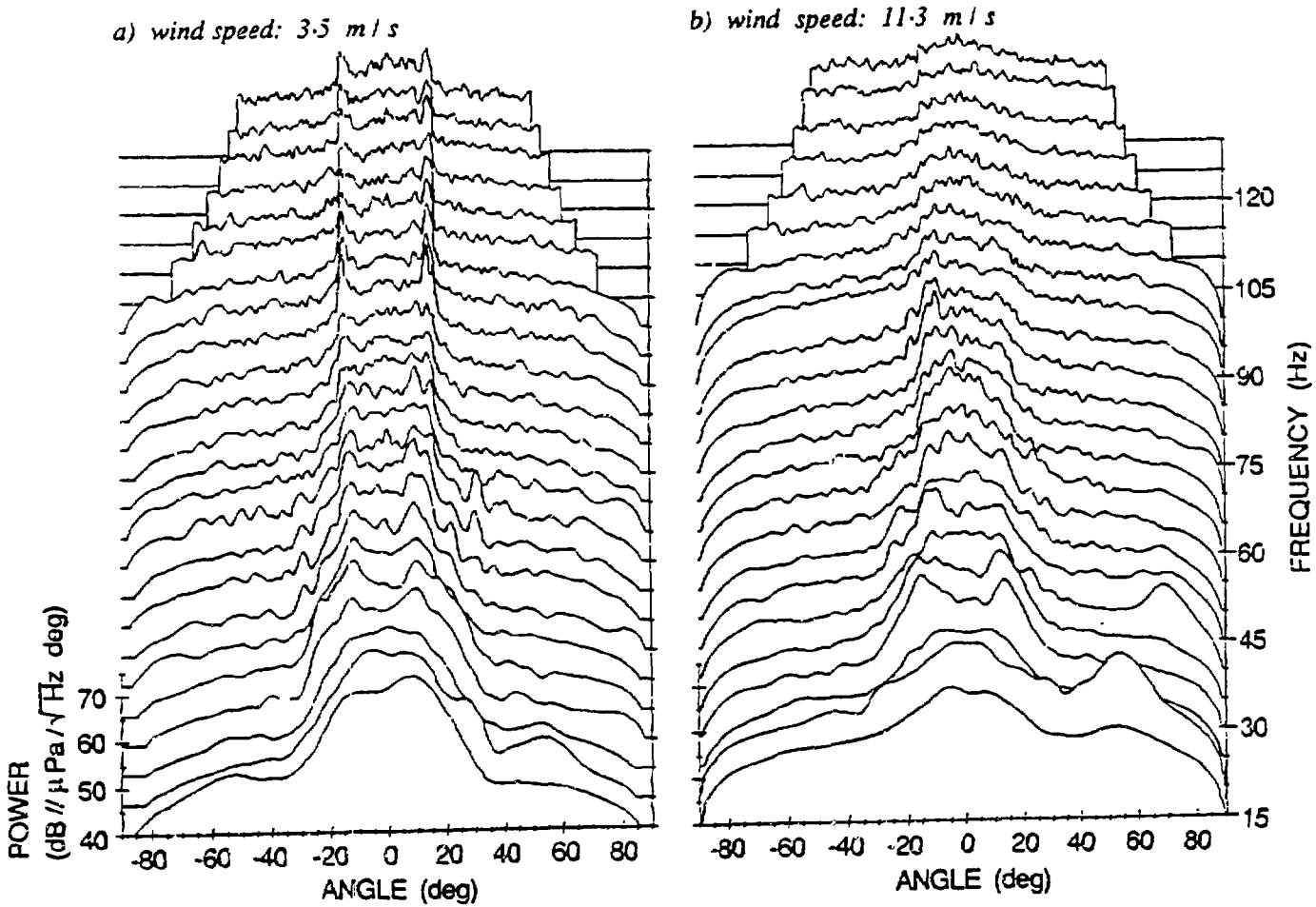

Figure 16 Spatial distribution of ambient noise as a function of wind speed. The spatial distribution for a (a) low wind speed (3.5 m/s) from data recorded on Julian day 258 at 0040 GMT and a (b) high wind speed (11.3 m/s) from data recorded on Julian day 258 at 1600 GMT, are displayed as a function of direction, frequency (every 5 Hz from 15 to 130 Hz) and power. The mid-array depth was at 850 m.

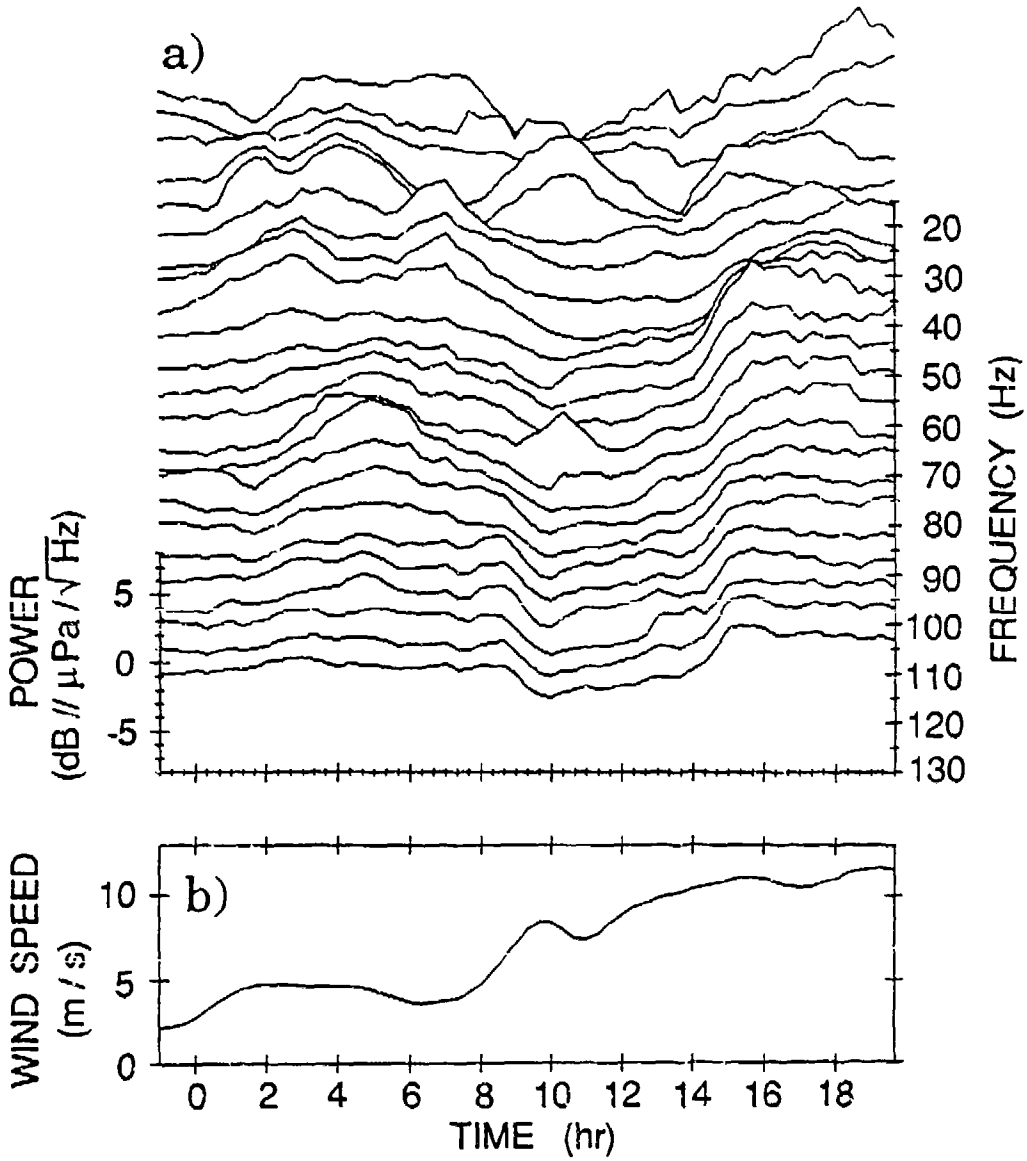

Figure 17 Spectral levels vs. time. The magnitude squared values from the 2 minute samples were averaged across the 2 minutes and then across selected channels giving one value for each frequency every 20 minutes for 21 hours. The averaged values were calibrated to dB//µPa/√Hz and the 21 hour mean for each frequency was removed to observe relative deviation from the mean value. The data smoothed slightly by a time-corrected running mean filter (n=4). Hourly wind speed estimates were smoothed by the same filter (Figure 19 shows the original unsmoothed version). The time axis represents GMT on Julian day 257/258.

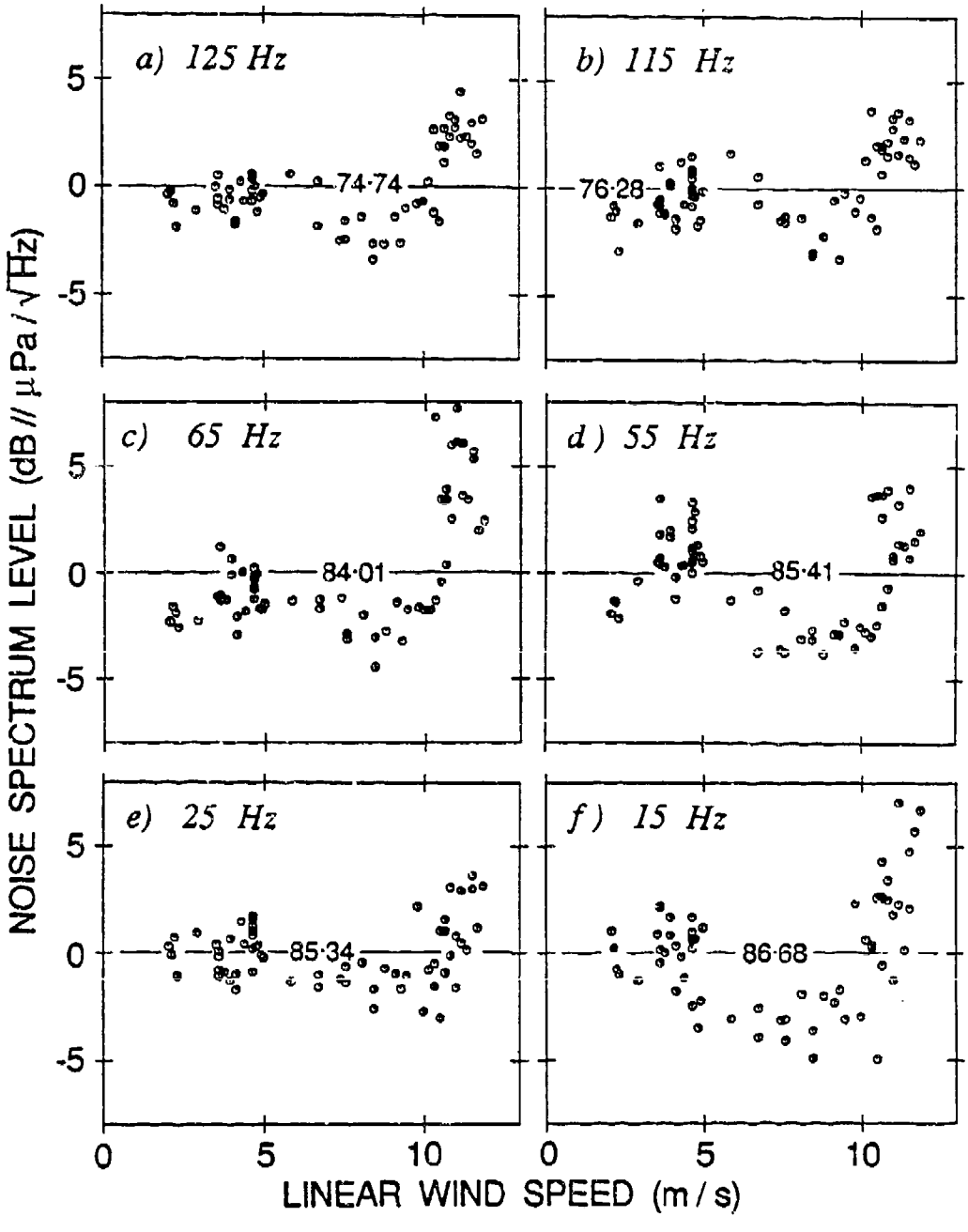

Figure 18 Spectral levels as a function of linear wind speed. Spectral levels at 6 different frequencies (2 low, 2 mid and 2 high) are plotted as a function of wind speed. Any quantitative relationship to wind speed must account for the relatively sparse and instantaneous estimates of wind speed. The specific frequency is notated in the corresponding panel. The number in each panel at the 0 dB mark is the normalization factor in dB//µPa/√Hz.

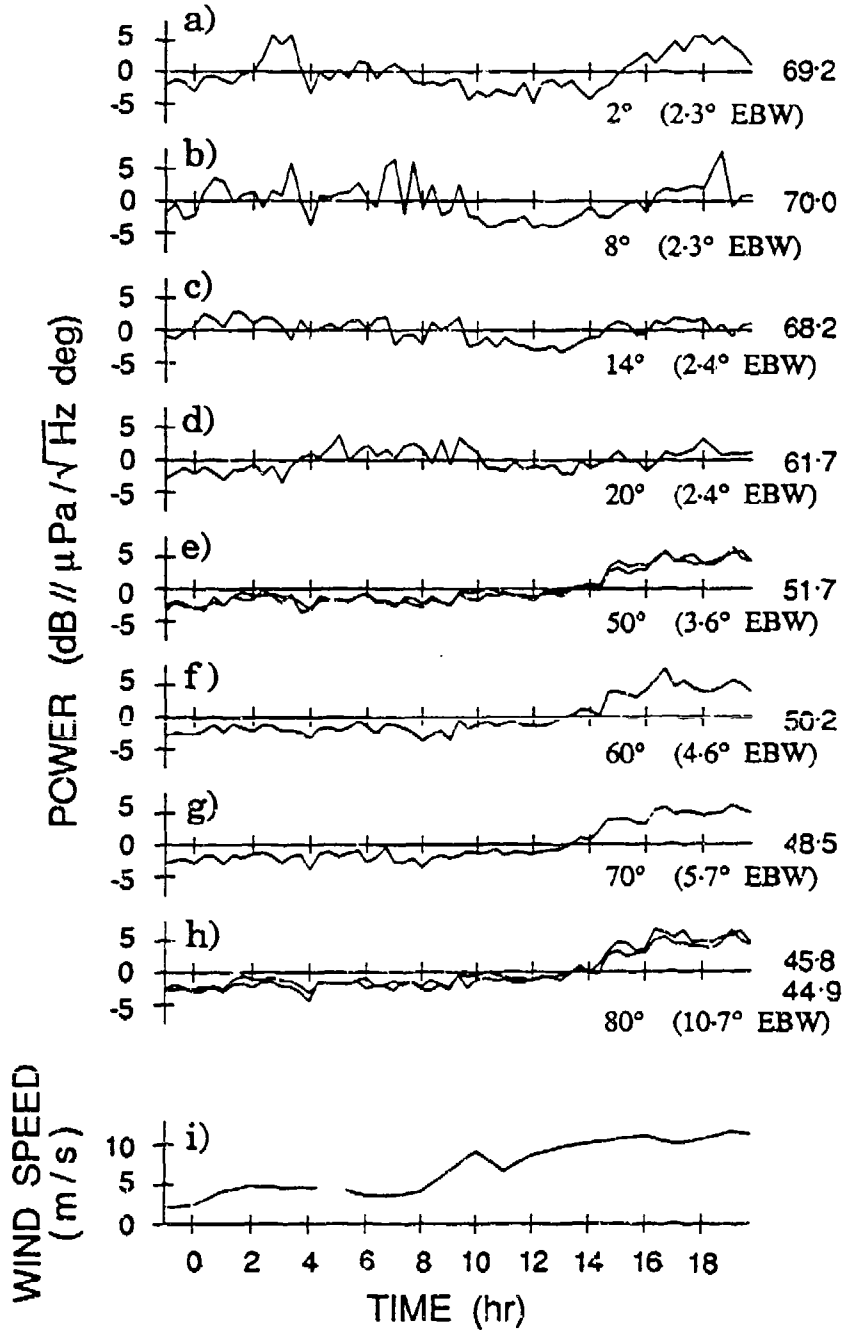

Figure 19 Directional time series. Specific beams are displayed with time at 55 Hz. The top 4 beams (2, 8, 14 and 20 °) are influenced by the ambient noise pedestal which is caused by distant sources. The bottom 4 beams (50, 60, 70 and 80°) are affected by local sources. Two downward looking beams (-50 and -80°) are also shown. The number to the right of the beam is the normalization factor (downward looking beam normalization factor below). The number after the beam direction is the EBW.

-80°. The mean difference is seen to be only 1 dB indicated to the right of the beam plots, increasing slightly at higher wind speeds for the 80° beam. The ray diagram corresponding to the 4 pedestal beams and the 50° beam is shown in Figure 13d. The decrease in spectral level between 1000 and 1400 GMT (Figure 17) is seen to be confined to the horizontal beams indicating that it is a distant effect. The presence of complicated bottom topography in the area of the hurricane track may account for the increase in horizontal beams at 1400 GMT which would reflect long distance variations. However without supporting data, changes in the distant shipping profile or energy from a high latitude storm cannot be discounted. However the increase in level at 1420 GMT is a local effect with the higher vertical angle levels increasing suddenly by as much as 5 dB. This effect is apparent at all frequencies and the abruptness of the change would indicate the onset of an additional source mechanism. The broad band frequency and spatial qualities of this change indicates that the mechanism is not system induced noise (array strum, *FLIP* noise). A second, broad band increase of smaller amplitude is seen at 1620 GMT which is more distinct at lower frequencies. Is this indicative of a change in source mechanism, for instance from spilling breakers to plunging breakers? Although preliminary simulations in the spectra of noise generated by breaking waves implies that plunging breakers drops off below 90 Hz [Papanicolaou and Raichlen, 1987], investigations in the area of wind induced noise mechanisms is in its infancy and future work may support the implications of the data presented here, that these noise mechanisms produce discrete changes in spectral values as opposed to a continuous function.

CONCLUSIONS

Prior to interpreting the ambient noise data, several factors relating to the quality of the data set were considered. The data were shown to be independent samples of a stationary Gaussian process for the time intervals used in the analysis. The impact of array calibration errors, sidelobe leakage, mechanical vibration and array shape was shown to be either negligible or predictable, affecting a isolated portion of the data set. Simulations indicated that for the majority of the data, measured spectral levels were not contaminated by array sidelobe leakage.

Ambient noise levels presented were reasonable for an area of high shipping density. The angular resolution of the array emphasizes the fact that much of the energy in the ambient noise pedestal is due to discrete sources (ships) which are smoothed by wider beams. Directional spectral levels did not vary significantly as a function of depth, not an unexpected result for the range of depths considered. Omnidirectional levels at low frequency are a function of processes besides local environmental changes thus directional data should be utilized in estimating wind induced noise levels.

Low frequency spatial distributions of ambient noise as a function of wind speed suggest more than one mechanism and display threshold type behavior observed previously [Carey, 1987]. The high wind speed domain (>10 m/s) demonstrated abrupt level changes, for beams outside the pedestal, corresponding to possible source mechanism onset, such as the commencement of

breaking waves, or a change in source mechanism such as the conversion from spilling breakers to plunging breakers. This hypothesis cannot be substantiated due to lack of supporting environmental measurements, however because the array data represent continuous samples of the noise field throughout the storm, the level changes are significant relative to the variability of the ambient noise field with time. These level changes, as much as 5 dB, were observed at all beam directions outside the ambient noise horizontal pedestal and at all frequencies processed between 15 and 130 Hz. The increase in absolute pedestal level and the increase observed in the near horizontal beams is a possible indication of downslope conversion of storm noise, but without azimuthal directivity, other possible mechanisms (coastal shipping variation, high latitude storm effects) cannot be ruled out.

ACKNOWLEDGEMENTS

A technical review of the manuscript by C. P. de Moustier and the valuable suggestions of V. C. Anderson, G. L. D'Spain and F. Fisher are gratefully acknowledged. Helpful references were provided by D. Farmer, A. Kibblewhite, D. Kewley and C. de Moustier. J. Griffith assisted with the illustrations and the captain and crew of the research platform *FLIP* contributed to the sea-going operation. This work was supported by the Office of Naval Research under Contract nos. N00014-87-K-0225 and N00014-87-C-0127.

REFERENCES

Anderson, V. C., "Arrays for the Investigation of ambient noise in the ocean," J. Acoust. Soc. Am., Vol. 30, pp. 470-477, 1958.

Anderson, V. C., "Variation of the vertical directionality of noise with depth in the North Pacific," J. Acoust. Soc. Am., Vol. 66, no. 5, pp. 1446-1452, Nov. 1979.

Arase, T. and E. M. Arase, "Deep-sea ambient noise statistics," J. Acoust. Soc. Am., Vol. 44, no. 6, pp. 1679-1684, 1968.

Axelrod, E. H., B. A. Schoomer and W. A. Von Winkle, "Vertical directionality of ambient noise in the deep ocean at a site near Bermuda," J. Acoust. Soc. Am., Vol. 37, no. 1, pp. 77-83, Jan. 1965.

Bannister, R. W. "Deep sound channel noise from high-latitude winds," J. Acoust. Soc. Am., Vol. 79, no. 1, pp. 41-48, Jan. 1986.

Bendat, J. S. and A. G. Piersol, *Random Data: Analysis and Measurement Procedures*, New York: Wiley Interscience, p. 124, 1971.

Berrou, J. L., O. Z. Bluy and R. A. Wagstaff, "A real-time system for towed-array calibration and performance analysis, or how to get 50 dB sidelobes from a towed array," CP-32, SACLANT ASW Research Centre, La Spezia, Italy, June 1982.

Bracewell, R. N. and J. A. Roberts, "Aerial smoothing in radio astronomy," Aust. J. Phys., Vol. 7, pp. 615-640, December 1954.

Bracewell, R. N., "Restoration in the Presence of Errors," Proc. IRE, Vol. 46, pp. 106-111, January, 1958.

Browning, D. G., N. Yen, R. W. Bannister, R. N. Denham and K. M. Guthrie, "Vertical directionality of low frequency ambient noise in the South Fiji Basin," NUSC Technical Document 6611, Naval Underwater Systems Center, New London, CT, 1982.

Burgess, A. S. and D. J. Kewley, "Wind-generated surface noise source levels in deep water East of Australia," J. Acoust. Soc. Am., Vol. 73, no. 1, pp. 201-210, January 1983.

Carey, W. M. and D. Browning, "Low frequency ocean ambient noise: measurements and theory," NUSC Technical Document 8175, Naval Underwater Systems Center, New London, CT, December 1987.

Carey, W. M., "Measurement of down-slope sound propagation from a shallow source to a deep ocean receiver," J. Acoust. Soc. Am., Vol. 79, no. 1, pp. 49-59, Jan. 1986.

Carey, W. M., R. A. Wagstaff, B. A. Brunson and M. R. Bradley, "Low-frequency noise fields and signal characteristics," NUSC Technical Report 131, Naval Underwater Systems Center, New London, CT, 1985.

Cavanagh, R. C. and W. W. Renner, "Vertical directionality and depth dependence of averaged acoustic signals and noise," J. Acoust. Soc. Am., Vol. 68, no. 5, pp. 1467-1474, Nov. 1980.

Crouch, W. W. and P. J. Burt, "The logarithmic dependence of surface-generated ambient-sea-noise spectrum level on wind speed," J. Acoust. Soc. Am., Vol. 51, no. 3, part 2, pp. 1066-1072, 1972.

Dashen, R. and W. Munk, "Three models of global ocean noise," J. Acoust. Soc. Am., Vol. 76, no. 2, pp. 540-554, Aug. 1984.

Fox, G. R., "Ambient noise directivity measurements," J. Acoust. Soc. Am., Vol. 36, pp. 1541-1564, 1964.

Hodgkiss, W. S. and F. H. Fisher, "Vertical directionality of ambient noise at 32° N as a function of longitude," Technical Memorandum 387, Marine Physical Laboratory, Scripps Institution of Oceanography, San Diego, CA, 1987.

Jobst, W. J. and S. L. Adams, "Statistical analysis of ambient noise," J. Acoust. Soc. Am., Vol. 62, no. 1, pp. 63-71, 1977.

McDonough, R. N., "Spectrum restoration for uniformly spaced arrays," J. Acoust. Soc. Am., Vol. 57, no. 4, pp. 913-922, 1975.

Middleton, D., "Acoustic modeling, simulation, and analysis of complex targets. II. Statistical evaluation of experimental data," ARL-TR-69-22, Applied Research Laboratories, University of Texas at Austin, Austin, TX, 1969.

Morris, G. B., "Depth Dependence of Ambient Noise in the Northeastern Pacific Ocean," J. Acoust. Soc. Am., Vol. 64, no. 2, pp. 581-590, Aug. 1978.

Morris, G. B., "Preliminary results on sea mount and continental slope reflection enhancement of shipping noise," SIO Ref. 75-34, Scripps Institution of Oceanography, La Jolla, CA, Nov. 1975.

Morse, P. M. and K. U. Ingard, *Theoretical Acoustics*, New York: McGraw-Hill Inc, p. 99, 120 and 178, 1968.

Papanicolaou P. and F. Raichlen, "Wave and bubble characteristics in the surf zone," NATO Advanced Research Workshop on Natural Mechanism of Surface-Generated Noise in the ocean, La Spezia, Italy, 15-19 June, 1987.

Press, W. H., B. P. Flannery, S. A. Teukolsky and W. T. Vetterling, *Numerical Recipes: the art of scientific computing*, Cambridge, England: Cambridge University Press, 1986.

Rudnick, P. and E. D. Squier, "Fluctuations and directionality in ambient sea noise," J. Acoust. Soc. Am., Vol. 41, no. 5, pp. 1347-1351, 1967.

Sotirin, B. J. and J. A. Hildebrand, "Acoustic navigation of a large aperture array," J. Acoust. Soc. Am., submitted in March 1989.

Sotirin, B. J. and W. S. Hodgkiss, "On array performance: A methodology of system calibration and noise identification," Technical Memorandum 410, Marine Physical Laboratory, Scripps Institution of Oceanography, San Diego, CA, March, 1989.

Sotirin, B. J. and J. A. Hildebrand, "Large Aperture Digital Acoustic Array," IEEE Journal of Oceanic Engineering, Vol. OE-13, No 4, pp. 271-281, Oct., 1988.

Tran, J-M. and W. S. Hodgkiss, "High resolution beamforming on vertical arrays in a realistic oceanic environment," Technical Memorandum 408, Marine Physical Laboratory, Scripps Institution of Oceanography, San Diego, CA, Jan. 1989.

Urick, R. J., *Ambient noise in the sea*, Washington, D.C.: Undersea Warfare Technology Office, Naval Sea Systems Command, Department of the Navy, 1984.

Wagstaff, R. A., "Low frequency ambient noise in the deep sound channel- the missing component," J. Acoust. Soc. Am., Vol. 69, no. 4, pp. 1009-1014, April, 1981.

Wagstaff, R. A., J. L. Berrou and F. D. Cotaras, "Use of the towship for assessing towed-array performance and analyzing data quality," J. Acoust. Soc. Am., Vol. 72, no. 3, pp. 983-992, September 1982.

Wagstaff, R. A., private communication, February 1988.

Wales, S. C. and O. I. Diachok, "Ambient noise vertical directionality in the Northwest Atlantic," J. Acoust. Soc. Am., Vol. 70, no. 2, pp. 577-582, August 1981.